MT-CWJCR-002-024

FINAL REPORT

MMS Project # 1435-01-01-PO-18216

FEASIBILTY OF THERMITE SPARKING WITH IMPACT OF RUSTED STEEL ONTO ALUMINUM COATED STEEL

Submitted to: Dr. Charles E. Smith
U.S. Department of Interior
Minerals Management Service
381 Eldon St., MS4021
Herndon, VA 20170-4817

Submitted by: Iman Maroef, Yeong-Do Park, and David L. Olson
Center for Welding, Joining, and Coating Research
Colorado School of Mines
Golden, CO 80401-1887

December 31, 2002

CSM

Center for Welding, Joining And Coating Research

Colorado School of Mines
Golden, Colorado 80401

TABLE OF CONTENTS

EXECUTIVE SUMMARY i

1. BACKGROUND 2

2. ALUMINUM COATING OF STEEL 4

2.1. Hot Dip Aluminum Coating 4

2.2. Types of Aluminum Coating on Steel 5

2.3. Aluminum-Zinc Alloy-Coated Steel 5

2.4. Aluminum Explosivity 6

3. CONSTITUTION OF RUST 7

4. INTRODUCTION TO THEORETICAL AND EXPERIMENTAL INVESTIGATIONS 9

5. PHASE 1: THERMODYNAMIC ANALYSES TO EVALUATE POSSIBLE REACTIONS FOR SPARKING 10

5.1. Thermochemical Calculations 10

5.2. Differential Thermal Analysis 11

5.3. Analysis and Interpretation of Thermodynamic Evaluations 16

5.3.1. Thermochemical Calculations and Differential Thermal Analysis 16

5.3.2. Energy State Necessary for Aluminum to React 17

5.3.3. Ignition of Thermite Reaction during Impact 17

5.3.4. Spallation of Liquid Aluminum Particles during Impact 18

5.3.5. Hydrogen Generation Due to Wet Thermite Mixture 20

5.4. Summary of Results of the Thermodynamic Evaluation 20

6. PHASE 2: IMPACT TESTING BETWEEN RUSTED/CLEAN PROJECTILE AND AL-COATED STEEL TARGET 22

6.1. Experimental Apparatus and Procedures 22

6.2. Preliminary Investigation of Impact Study 24

6.3. Main Investigation of Impact Study 29

6.4. Results of the Main Impact Study 32

6.5. Discussion of the Impact Study 38

6.6. Summary of the Impact Study 41

7. PHASE 3: COMBUSTION TESTING UPON IMPACT BETWEEN RUSTED PROJECTILE AND AL-COATED STEEL TARGET 43

7.1. Experimental Apparatus and Procedures 43

7.2. Experimental Design for Combustion Study 49

7.3. Results on the Combustion Study 49

7.4. Discussions and Verification Tests on the Combustion Study 57

7.5. Summary of Combustion Study 61

8. CONCLUSIONS 62

APPENDIX A : HARDWARE A1-A4

APPENDIX B : SPARK IMAGES B1-B7

APPENDIX C : PROJECTILE VELOCITY MEASUREMENT C1-C3

1. BACKGROUND

The use of aluminum-coated steels in a marine atmosphere is a concern, as seen from ABS reports (1), UK Health and Safety Laboratories reports (2), DNV reports (3-5) and the open literature (6-12). Hay and Adarmann have reported an excellent historical overview on thermite sparking (10). The issue focuses on the impact of rusted steel on aluminum or vice versa. It has been hypothesized that, upon impact, the intimate contact between aluminum and rust will result in an exothermic reaction producing aluminum oxide, water and iron. It has also been hypothesized that this reaction will generate sufficient heat to cause a spark. Rae (12) suggests that the aluminum smearing onto rust was the most likely mechanism if thermite spalling occurs.

The primary basis for this thermite sparking issue are the reported explosions in coal mines due to the use of aluminum in mining machinery (11). On aluminum contact with various corrosion and/or environmentally-produced surface products, it has been reported that sparking has occurred, in turn producing a gas explosion. It is improbable that the surface product, called "fire damp," is rust, but rather a mixture of rust and a carbon source (11). The sparking of steel during grinding and the spatter during welding are directly related to the amount of carbon available to generate CO and CO_2. The fire damp mixture, with its carbon association, may be a potential problem in coal mines but does not correlate to rusted steel with aluminum contact in a marine environment.

Friction sparking, which is the result of the rubbing of two surfaces, leads to the potential production of a spark. It has been suggested for aluminum that thermite sparks are more likely to occur than friction sparks, because aluminum is a metal that does not produce sparks on grinding. This non-sparking feature is used to sort and distinguish aluminum from other metals and alloys (13, 14).

Drop tests, in which a rusted steel plate is dropped onto aluminum and aluminum alloy-coated steel with varying coating thicknesses, have been performed by Nippon Steel (8). The dropping of rusted steel onto a rusted steel plate was included in this investigation for comparison. These impacts were performed in an enclosure containing an explosive gas mixture. Of the twenty drops of the rusted steel onto rusted steel, twenty percent produced explosions. However, only thirteen percent of the sixty drops of the rusted steel onto aluminum-coated steel resulted in an explosion. This observation suggests that the thermite contribution to sparking does not enhance the friction sparking common between steel impacting steel. The aluminum surface may even hinder the frictional sparking behavior.

Hyundai Heavy Industries has also performed similar drop test of rusted steel onto hot dip aluminized steel (6). These tests were performed in a chamber containing a 4-5 pct. propane gas in air mixture. No explosions were found with twenty tests. The rusted steel weighed 48 Kg and was dropped 10.5 meters, resulting in an impact energy of 500 Kg·m. They also reported an air temperature of 14°C and humidity of 74 percent.

Ramberg reviewed the concerns regarding the use of aluminum in the marine industry and he reported on the probability of ignition of explosive gases when aluminum and steel impact rusted steel (3). He noted that the findings of Foyn and Moe (7) indicate a considerably higher probability of ignition of rusted steel impacting aluminum than of impacting steel. With Foyn and Moe's test arrangement and procedures, no ignition was

reported for rusted steel impacting steel. Also, the measure of probability of ignition of rusted steel impacted on aluminum was even smaller than previously reported by other investigators.

Ramberg (3) also reported that a detailed safety analysis, considering all relevant aspects related to the safety of aluminum in marine structures, concludes that the thermite reaction does not represent an unacceptable hazard. The thermite reaction is only one of a great number of possible ignition sources and its importance should not be exaggerated in comparison to other sources.

2. ALUMINUM COATING OF STEEL

Aluminum coatings on steel offer structural and component functional advantages in both mechanical integrity and corrosion resistance (15,16). The marine industry uses steel for its properties, formability and weldability, resulting in economy. The metallic aluminum coating insulates the steel from the marine environment and, when wet, serves as a sacrificial anodic surface to protect exposed steel. The aluminum coating of the steel is especially useful for corrosion resistance in a corrosive atmosphere. In this situation the mechanism for protection is the passive aluminum oxide film. If the aluminum oxide barrier is breached, such as occurs in environments containing chlorides, the aluminum can electrochemically prevent the steel from rusting. Aluminum coatings have been reported to protect 1.3 to 2.2 times longer than galvanized (zinc) coatings of the same thickness in industrial and marine atmospheres.

The mechanism for corrosion resistance is that the oxygen reacts to form the protective aluminum oxide layer. Other environmental reagents can also assist in the formation of a protective passive film. An amorphous hydrated aluminum sulfate corrosion product has been identified, suggesting that SO_2 is an important factor in atmospheric corrosion.

Aluminum-coated steel is not generally used where it is in continuous contact with an aqueous corrosive environment. It is reported that aluminum-coated steel is not used in seawater (15,16). It is not that the coating does not protect, but that the aluminum corrosion rates are too high to provide economical use. Aluminum coatings have been used as part of a more complex corrosion protection system.

Aluminizing steel has more processing difficulties than the galvanizing process due to the high melting temperature and vaporization temperature, but aluminum-coated steel is readily available throughout the world. Major uses of this product include roofing panels, automotive exhaust components, chain fence, fasteners, aerospace fuel and pneumatic line fittings, electrical connectors, and electrical black boxes.

2.1. Hot Dip Aluminum Coating

Aluminizing is the process of applying a hot-dipped aluminum coating to steel (17). Batch and continuous aluminum hot-dipping processes are both performed. The typical process steps consist of cleaning, heating, fluxing, and coating. The cleaning of the steel surface involves a series of steps: an alkaline cleaning and water rinse, descaling by abrasive blasting or acid pickling, followed by rinsing and drying. Any oxide left after the cleaning step is dissolved by fluxing in a 600°C molten-salt bath with an immersion time ranging from thirty seconds to several minutes. Immediately after fluxing, the steel is immersed in a molten aluminum bath at 700°C. The thermal process (temperature and immersion time) must be carefully controlled to attain an acceptable coating thickness. Related steps can be achieved by continuous in-line equipment which is used for steel strip, sheet or tubing.

Flame and plasma spray are also used to deposit aluminum coatings onto steel (18). Aluminum coatings have also been deposited on small parts with vapor and ion plating processes. The vapor and ion plating processes are not very useful for the larger parts required by marine use and do not offer any economical advantages.

2.2. Types of Aluminum Coating on Steel

Aluminum coatings are primarily of two types (15-18). Type 1 uses an aluminum alloy containing five to eleven wt. pct. silicon, which is a hypoeutectic alloy offering lower melting temperatures than pure aluminum. Type 2 uses commercially pure aluminum for the coating. The Type 2 coating microstructure results in a layer of aluminum, often with a smaller internal layer of iron-aluminum intermetallic (Fe_2Al) phase adjacent to the steel. With some processes, additional iron-aluminide phases have been identified. This intermetallic phase formed during processing is brittle and will fracture during formation. The growth of the Fe_2Al layer has been retarded by alloy addition, such as copper or beryllium. As with other sacrificial coatings, the thickness of the coating is more important than any coating defects, such as very localized steel exposure. Compared to galvanized coatings, aluminum coatings require moderate thickness to avoid problems from the increase of coating defects associated with the higher processing temperature.

The two types of aluminum coatings do show a distinct difference as seen in the darkening and pinpoint rust formation that occurs very early on Type 1 coatings, resulting in an appearance factor. The weight loss for both coatings is approximately the same. Type 1 coatings are generally used for high temperature applications, such as automotive exhaust components. Type 2 aluminum coating is primarily used for atmospheric corrosion resistance.

Thickness loss of a Type 1 aluminum coating is approximately 200 μm (7.8 mils) after immersion in seawater for a year. Type 2 aluminum coatings for the same conditions experienced 38 μm (1.5 mils) loss in coating thickness. After fifteen years in atmospheric exposure, Type 2 aluminum coatings have experienced thickness losses as low as 5 to 7 μm (0.20 to 0.26 mils).

In certain environments, aluminum coatings cannot provide cathodic protection to exposed steel, resulting in the occurrence of rust at coating defects and cut edges. This rusting seldom progresses but may be an important appearance consideration. Aluminum coatings have been subject to crevice corrosion in marine environments.

2.3. Aluminum-Zinc Alloy-Coated Steel

To improve the metallic coating resistance, the combination of aluminum and zinc is used as a high alloy coating (55 wt. pct. Al, 43.4 wt. pct. Zn – 1.65 wt. pct. Si). The volume percent is approximately 80 vol. pct. aluminum and silicon and 20 vol. pct. zinc. The coating exhibits a two-phase microstructure of cored aluminum-rich dendrites and a zinc-rich interdendritic constituent. This coating is bonded to the steel with a thin $Al_{13}Fe_4$ intermediate layer (48 wt. pct. Al, 24 wt. pct. Fe, 14 wt. pct. Zn and 11 wt. pct. Si). Silicon particles are often found in the interdendritic region.

The aluminum-zinc alloy coatings were not metallurgically feasible until it was discovered that silicon inhibits the rapid growth of the intermetallic phase during hot-dipping. The 55Al-Zn coatings offer both a passive film barrier and galvanic protection. Any break in the coating resulting in localized steel exposure will be protected because of the intimate contact of the zinc. The aluminum-zinc alloy coatings are used for metal roofing, automotive components, appliances and corrugated steel products. The 55Al-Zn alloy is most likely to produce corrosion resistance between galvanized and aluminum

coatings. Supplemental corrosion protection would be required for long term use in seawater. The application of 55 Al-Zn the coatings is increasingly used in industry.

2.4. Aluminum Explosivity

Aluminum reacts with moisture or free oxygen in the air. This reaction results in a thin, normally protective, oxide layer, which inhibits further reaction by keeping the reagents separated. In powder form, where the ratio of area to volume can be very large, the chemical activity of aluminum is more significant, making sparking possible (19-21). The resulting oxide contents for these particles are a function of particle size and can range from 0.1 to 1.0 wt. pct.

The explosivity of aluminum particles as a function of size is given in Table 1. Coarse particles over 200 mesh are very difficult to ignite. Particles with sizes in the range of –200 to +325 mesh tend to be explosive, even in relatively small concentrations. Severe explosive characteristics are exhibited by particles with sizes less than –325 mesh. The ignition temperature generally reduces as the particle size reduces. The effect of aluminum particle size on the susceptibility to explosion is also shown in Figure 1. The U. S. Bureau of Mines (19) reports the following characteristics of aluminum powder explosivity: a minimum concentration of 0.045 Kg/m^3, a minimum ignition energy of 50 mJ (0.012 cal), a ignition temperature of an aluminum particulate cloud of 650°C, an ignition temperature of a particle layer of 760°C, a maximum explosive pressure of 503 Kpa and a maximum rate of pressure rise of 140 Mpa.

The explosivity is also influenced by the aluminum particle shape because flake shapes offer an even greater surface-to-volume ratio and have a greater tendency to ignite than atomized particles. Also, the presence of moisture generally tends to increase the potential of aluminum powder pyrophoricity.

3. CONSTITUTION OF RUST

Hydrous ferrous oxide ($FeO \cdot nH_2O$) or ferrous hydroxide ($Fe(OH)_2$) make up the diffusion barrier layer next to the iron surface through which O_2 must diffuse (22). Ferrous hydroxide is a fairly strong base with a pH of about 9.5. This situation results in an alkaline condition for the iron surface exposed to aerated water. The color of ferrous hydroxide, which is white when pure, is most often seen as green to greenish black because of incipient oxidation by air. The outer surface of this protective film, with its more direct exposure to oxygen, converts ferrous hydroxide to ferric hydroxide. When the hydrous ferric oxide ($Fe(OH)_3$) is heated it loses all its water and yields the anhydrous oxide Fe_2O_3. This oxide exists in a variety of crystallographic forms. The form depends on the method by which it was produced. When this oxide is heated above 1000°C, when iron burns in oxygen, or when it is heated in steam, the result is the formation of Fe_3O_4 (magnetite).

Hydrous ferric oxide ($Fe(OH)_3$) is orange to red-brown in color and is the chemical nature of ordinary rust. The αFe_2O_3 has a greater negative free energy of formation; it is more stable than γFe_3O_4. Saturated $Fe(OH)_3$ has a pH of approximately 7. A magnetic hydrous ferrous oxide, $FeO \cdot nH_2O$, often is found as a black intermediate layer between hydrous Fe_2O_3 and FeO. The overall result is that rust films are composed of three layers of iron oxide in different states of oxidation. After water evolution or hydroxide decomposition, the resulting rust exists as either nonmagnetic αFe_2O_3 (hematite) or magnetic γFe_3O_4.

Table 1. Size of spalled particle that will allow ignition to form Al_2O_3 (not a thermite reaction). Particle size below 149 μm (100 mesh) has an ignition temperature of 760 °C (2). This is 100 °C above melting of aluminum (20).

Power mesh fraction	Lower explosive limit(a) oz/ft^3	Relative explosibility
-40+100	No ignition	None
-100+140	No ignition	None
-140+200	No ignition	None
-200+270	0.111	Strong
-270+325	0.090	Strong
-325	0.045	Severe

(a) Values for Kilograms per cubic meter are exactly the same.

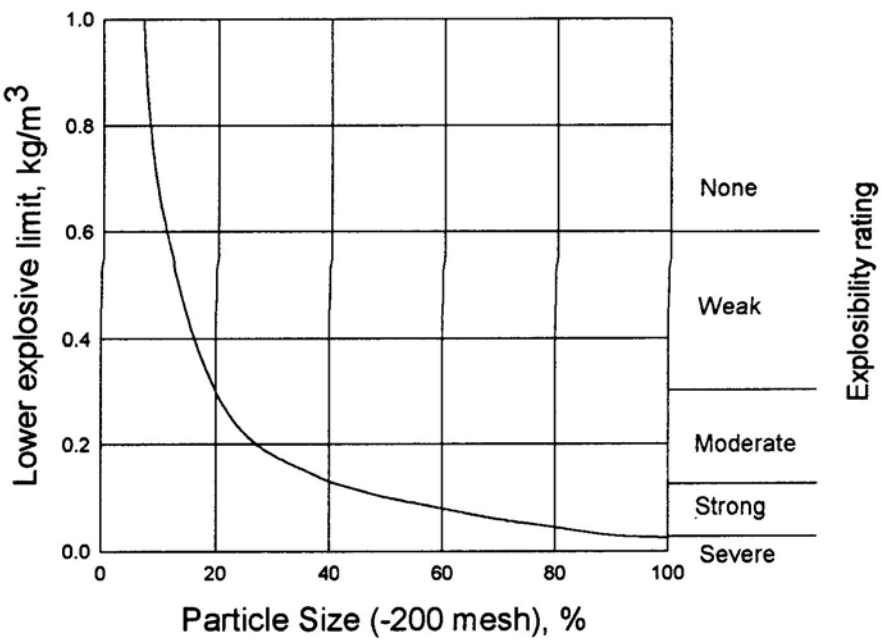

Figure 1. Effect of aluminum powder particle size on explosibility shown by comparing lower explosion limit with the percentage of particles less than 200 mesh in size (20).

4. INTRODUCTION TO THEORETICAL AND EXPERIMENTAL INVESTIGATIONS

The investigation of the fire hazard potential due to impact between a rusted steel object and Al-coated steel has been conducted in three phases. Briefly, these phases can be summarized as follows:

1. Phase 1: Thermodynamic analyses to evaluate possible reactions for sparking. In this phase, differential thermal analyses (DTA) were conducted on different conditions of rust (and iron oxide), mixed with aluminum powder, to identify their respective exothermic reaction temperature. Further, the DTA data was used to evaluate the potential of these different rusts for sparking on established impact tests through fundamental thermodynamic calculations. From the samples of rust or oxides investigated, dry rust showed the highest potential for sparking.
2. Phase 2: Impact testing between rusted/clean projectile and Al-coated steel target. In this phase an experimental apparatus was constructed to allow for impact testing between rusted steel object with Al-steel target at a wide range of impact energy. Threshold values for sparking for selected rust and target conditions were identified in the light of photographic/video documentation and photodiode light sensing. Threshold impact energies were also determined through projectile velocity measurements by high-speed camera and through impact energy assessment with the pendulum method.
3. Phase 3: Combustion testing upon impact between rusted projectile and Al-coated steel. In this phase, the combustion potential of successful spark generations upon impact incidents were evaluated in the presence of various combustible mixtures. This phase included upgrading the capability of the experimental apparatus constructed in phase 2. Various ratios of mixture between flammable gas and air were prepared within a combustion chamber where spark generation took place by impact. In addition, an environment containing gasoline liquid and vapor was also investigated.

5. PHASE 1: THERMODYNAMIC ANALYSES TO EVALUATE POSSIBLE REACTIONS FOR SPARKING

5.1. Thermochemical Calculations

Five exothermic chemical reactions were evaluated for their ability to generate heat. Three reactions (reactions 1, 2, and 3) are the classical thermite reactions involving iron oxides with aluminum. There are three iron oxides: hematite (Fe_2O_3), magnetite (Fe_3O_4), and wustite (FeO). Hematite offers the largest amount of heat per mole of oxygen and wustite offers the least. Commercial thermite reagents have been defined in the literature as either a Fe_2O_3-aluminum or a Fe_3O_4-aluminum mix.

Equation 1

$$2Al + Fe_2O_3 = Al_2O_3 + 2Fe$$
$$\Delta H_1 = -204 \text{ Kcal}$$

Equation 2

$$8Al + 3Fe_3O_4 = 4Al_2O_3 + 9Fe$$
$$\Delta H_2 = -818 \text{ Kcal}$$

Equation 3

$$6Al + 9FeO = 3Al_2O_3 + 9Fe$$
$$\Delta H_3 = -636 \text{ Kcal}$$

Iron rust is a hydrous iron oxide or iron hydroxide. There are two iron hydroxides: ferrous hydroxide ($Fe(OH)_4$) and ferric hydroxide ($Fe(OH)_3$). Rust is a layered structure that often has a layer of both hydroxides but is usually primarily ferric hydroxide. The reactions 4 and 5 involve the reactions of these two hydroxides with aluminum. Reaction 4 is probably the best description of a hydroxide thermite reaction. The heat generated by the reactions was calculated.

Equation 4

$$2Al + 2Fe(OH)_3 = Al_2O_3 + 3H_2O + 2Fe$$
$$\Delta H_4 = -181 \text{ Kcal}$$

Equation 5

$$2Al + 3Fe(OH)_2 = Al_2O_3 + 3H20 + 3Fe$$
$$\Delta H_5 = -167 \text{ Kcal}$$

The heats of formation for the reactants and products are given in Table 2. The heat of reactions for the above equations is given in Table 3. These calculations were made at standard temperature and pressure; for this application they are expected to produce good

heat values for comparison. Table 3 also reports the heat of reaction as a function of oxygen content, as a function of aluminum content, and as a function of iron content. The heat as a function of oxygen content (from an oxide or hydroxide) probably offers the best values for comparison for heat generation by these various reactions.

Table 2. Heat of Formation (in kcal/mol)

COMPOUND	K Cal/mole	DESCRIPTION
a) $Fe(OH)_3$	-197.37	Ferric hydroxide (rust)
b) $Fe(OH)_2$	-135.87	Ferrous hydroxide
c) Fe_2O_3	-200	Ferric oxide
d) Fe_3O_4	-265.95	$FeO \bullet Fe_2O_3$ spinal
e) FeO	-64.04	Ferrous oxide
f) Al_2O_3	-404	Aluminum oxide
g) H_20	-57	Water

Table 3. Thermochemical calculations of the various heats of reactions for the exothermic reactions involved

R_x	Identify Oxide Rust	H_o (Kcal)	H_o/[O] (Kcal)	H_o/[Fe] (Kcal)	H_o/[Al] (Kcal)	H_o/[Al_2O_3] (Kcal)
1.	Oxide	-204	-68	-102	-102	-204
2.	Oxide	-818	-68	-91	-102	-204
3.	Oxide	-636	-71	-71	-106	-212
4.	Rust	-181	-30	-90	-90	-181
5.	Rust	-167	-24	-53	-84	-167

5.2. Differential Thermal Analysis

Differential thermal analysis (DTA) was performed on three samples:

1) aluminum and hematite powder mix (thermite),
2) aluminum and moist $Fe(OH)_3$ mix,
3) aluminum and air-dried $Fe(OH)_3$ mix.

All DTA runs were made in air with a heating rate of 20°C/min, heating the sample from room temperature to 1400°C. Figure 2 shows the DTA result of the classical thermite mixture of aluminum powder and hematite. The curve has three indications of phase transitions and reactions. The endothermic dip at 660°C (indication 1) correlates well with the melting temperature for aluminum. The rise at 1100°C

(indication 2) corresponds to the thermite (exothermic) reaction as reported in the literature (23). The large rise at 1350°C is expected to be the oxidation of the excess aluminum. Notice that the thermite reaction has occurred at 450°C above the melting temperature for aluminum and that hematite has been in direct contact with the liquid aluminum during this temperature range without reacting.

Figure 3 shows the DTA results of ferric hydroxide and aluminum powder mix that has excess moisture, a situation common to exposed rust. This test was run due to a report (23) that a significant hazard in the thermite reaction results from contamination from moisture. During the thermite reaction at 1100°C, water is reduced and hydrogen evolved. This situation can produce an explosive mixture with the surrounding air. With the ramping of the temperature, the first dip around 150°C (indication 1) represents the endothermic behavior in driving off the excess moisture. The dip at 660°C (indication 2) is due to the latent heat necessary to melt the aluminum powder. There is no indication of significant exothermic (heat-generating) reactions with wet rust.

Figure 4 shows the DTA results of air-dried ferric hydroxide and aluminum powder that has excess aluminum. With the same ramping (heating) rate, the first dip at approximately 150°C (indication 1) is associated with driving off excess water. The rise at 330°C (indication 2) is related to some chemical reaction heating source, possibly of a small transformation associated with the various phases making up rust. The dip at 660°C (indication 3) represents the melting of the powder aluminum. The exothermic reaction at 900°C (indication 4) is the reaction of interest between ferric hydroxide and aluminum that generates heat. It occurs 240°C above the melting temperature of aluminum. During the ramping through this temperature range, the ferric hydroxide is in direct contact with liquid aluminum and did not react until approximately 900°C. There is another small endothermic reaction at 1130°C (indication 5) which is unexplained but which requires or consumes heat. The exthermic reaction at approximately 1370°C (indication 6) is most likely reporting the oxidation of the excess liquid aluminum.

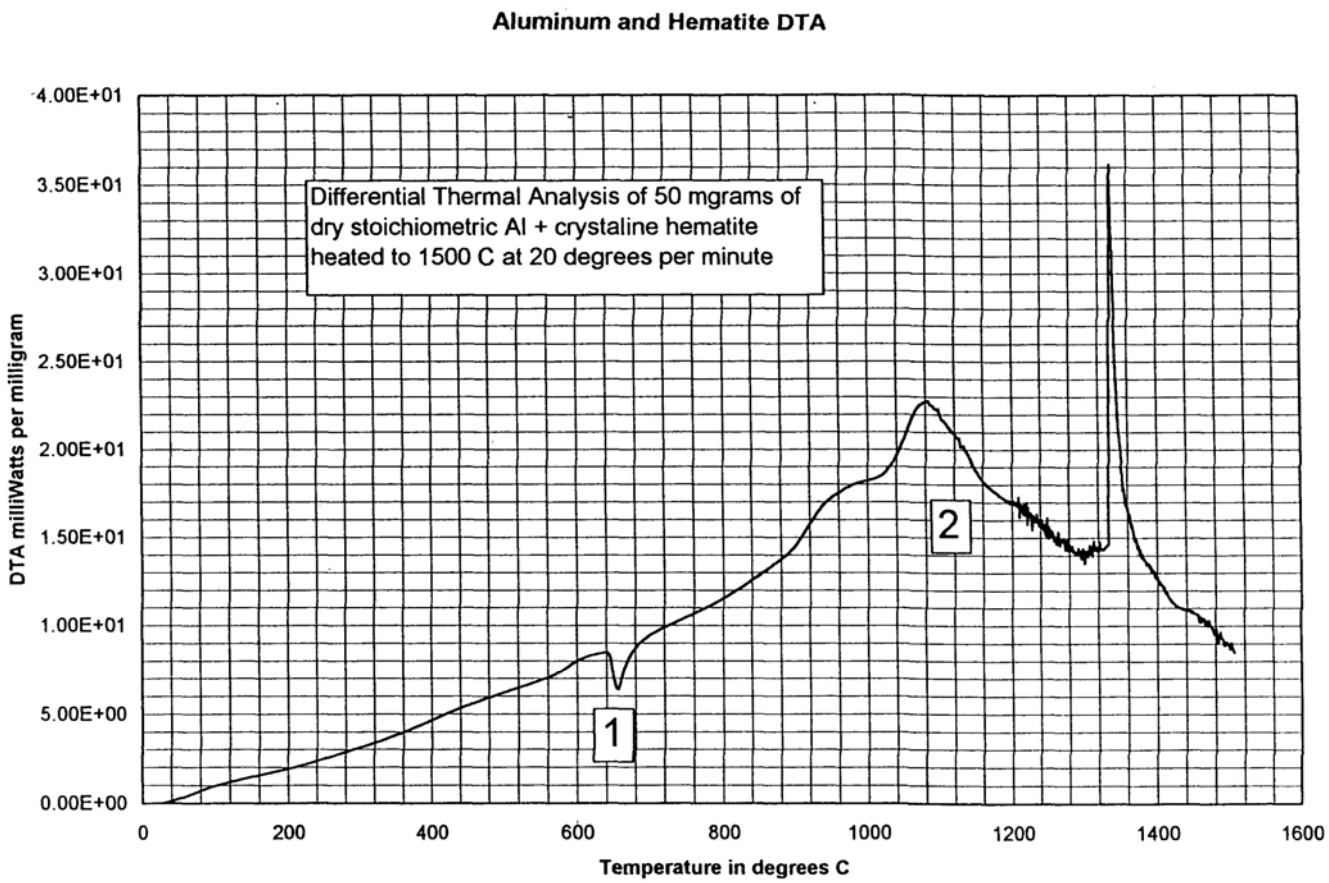

Figure 2. Differential Thermal Analysis of a mixture of aluminum and hematite (Fe_2O_3)

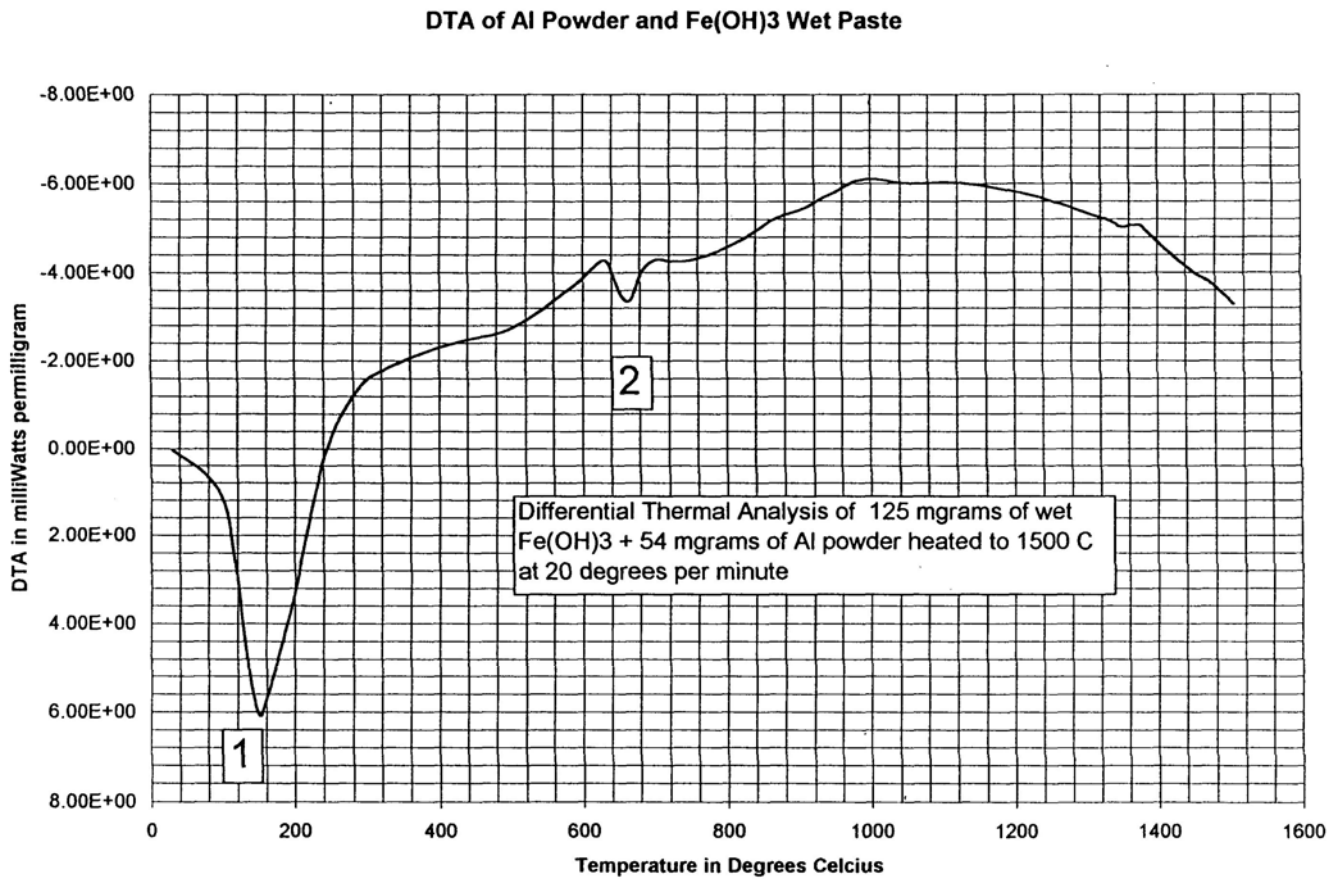

Figure 3. Differential Analysis of a mixture of aluminum and moist rust)

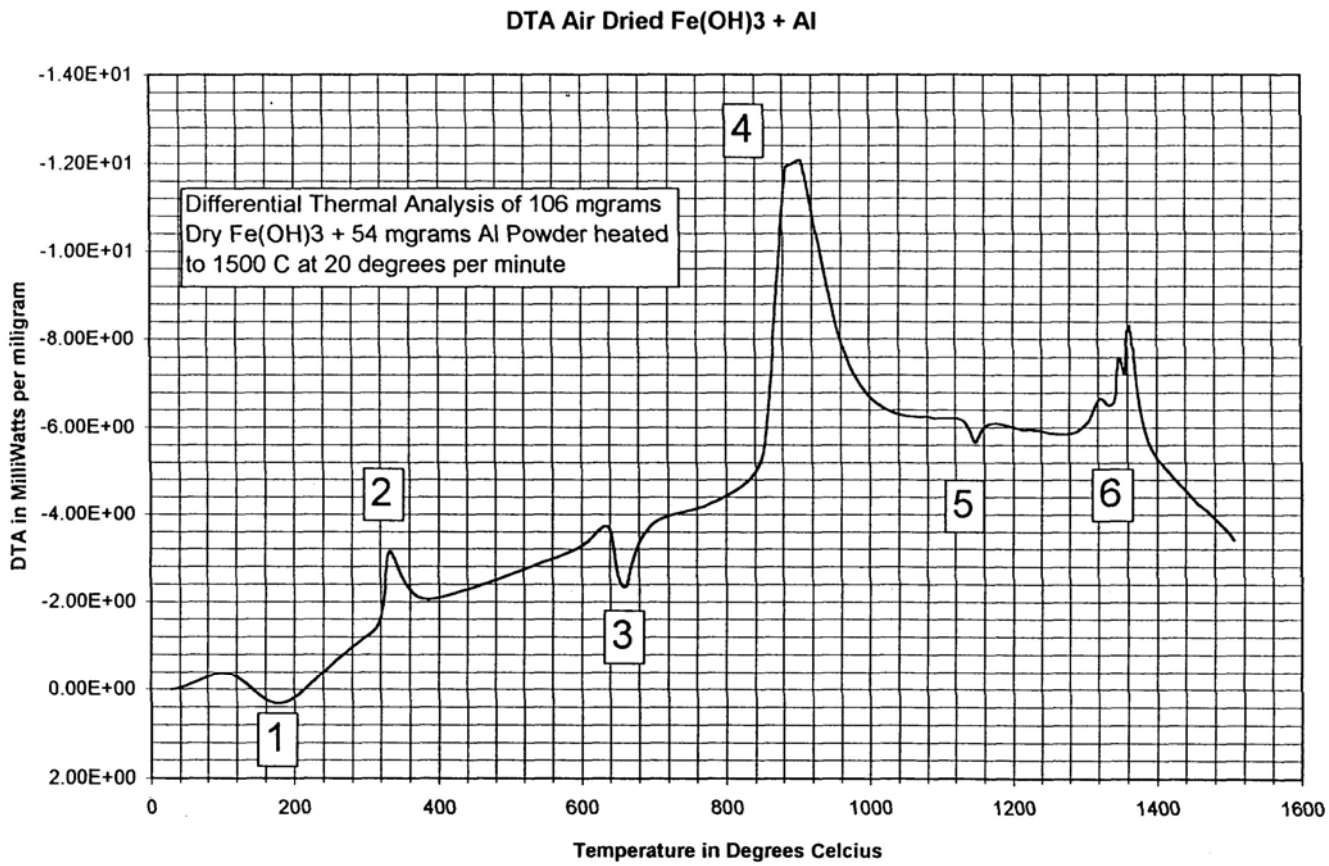

Figure 4. Differential Thermal Analysis of a mixture of aluminum and air-dried ferric hydroxide.

5.3. Analysis and Interpretation of Thermodynamic Evaluations

The previously reported results of other investigations of drop testing rusted steel impacting onto aluminum, or vice versa, were evaluated to identify collected observations of the results and to provide for a more sound base from which to draw a conclusion. The drop testing of a rusted steel plate onto an aluminum plate within a container housing an explosive gas mixture was the procedure used to evaluate sparking, regardless of whether it was friction sparking or thermitically enhanced friction sparking. The three investigations each had their own weight and height for the drop specimen, causing a variation in impact energy. Table 4 lists the impact energies investigated with drop testing by the various investigators. Even with this range of input energies, there is no overall evidence of a higher frequency of explosion for the aluminum to rusted steel event as compared to steel impacting on rusted steel.

Table 4. The magnitude of impact energies for various reported drop tests

Investigator	Impact Energy
Al on Rusted Steel	32-64 Kg.m
Steel on Aluminum	144 Kg.m
DNV	700 Kg.m

There is some indication in one investigation that the aluminum coating may even hinder the sparking-explosion events. There was some reporting that wet industrial thermite mixtures have a problem with hydrogen generation during the thermite reaction. The hydrogen, if collected, has been reported to explode (23). The amount of hydrogen that would be generated during the time of impact is very unlikely to cause a microexplosion. There was no significant DTA exothermic peak suggesting a hydrogen reaction event.

5.3.1. Thermochemical Calculations and Differential Thermal Analysis

A thermochemical calculation was performed for aluminum reacting with the three different oxides of iron and also on the two different hydroxides or hydrous iron oxides, which compose rust. From these calculations and by comparing rust-aluminum reactions to iron oxide-aluminum reactions, the amount of heat produced per mole of oxygen from the oxide or rust was found to be less than half for the rust reaction when compared to the typical thermite reaction. It appears that the hydrous iron oxide (rust) changed the energetics so that the exothermic contribution was significantly reduced.

Differential thermal analysis was performed to evaluate the sequence of chemical reactions associated with the ramp heating of a mixture of air-dried rust-aluminum powder, moist rust-aluminum powder, and iron oxide-aluminum powder. The results indicate that in all cases the rust or oxide is in intimate contact with molten aluminum to at least 240°C above the melting temperature of the aluminum before the exothermic reaction occurs. The degree of intimate contact in molten aluminum must be at least equivalent to aluminum smears on rusted steel. These results suggest that very high temperatures must be reached before the thermite-type reaction would occur. In industry

practice, the thermite mixture used in welding needs to be initiated using a burning magnesium strip embedded into the mixture.

5.3.2. Energy State Necessary for Aluminum to React

A method to determine the thermally activated state for ignition of the aluminum exothermic reaction can be developed by measuring thermite temperature as seen from the differential thermal analysis (Figures 2,3 and 4) and then reporting the enthalpy of aluminum at this temperature. This thermal state means that statistically there are sufficient aluminum atoms to have sufficient energy to surmount the activation energy barrier for the reaction to proceed. Table 5 gives the measured temperatures for Al-Fe_2O_3 and Al-dry rust $Fe(OH)_3$ mixtures, and the energy (heat) of the aluminum at those temperatures. These energy values will be used as the energy barriers that must be surpassed by the mechanical (shock) interaction. Because the height and weight of the drop specimens are known, the drop energy can be calculated. Assuming that the interaction of the rusted steel drop specimen with the aluminum plate occurs instantaneously, there is insufficient heat transfer to allow impact energy to travel any distance into the aluminum. Also, an assumption of no plastic deformation during the interaction is used, resulting in a worst case scenario for localization of energy. This worst case "impact energy" value is compared with the reported activation energy. Applying reasonable boundary conditions for the dimensions of the aluminum involved with this very localized interaction, the drop specimen's weight and height can be estimated for achieving a thermite reaction and the conditions for spalling of liquid aluminum particles can be calculated.

Table 5. Energy barrier for thermite reaction

Combination	Reaction Temp (°C)	Reaction Temp (°K)	ΔH_T (mole) for Al, (cal) 100 cm^3X0.1cm at rx Temp.	ΔH_T (0.01mole) (cal) for (1cm2X0.1cm) $1cm^3$
Al-Fe_2O_3 Literature	1100	1373	10245	102.45
Al-Fe_2O_3	1080	1373	10053	100.53
Al-wet rust	1000	1273	9484	94.84
Al-dry rust	900	1173	8725	87.25

5.3.3. Ignition of Thermite Reaction during Impact

The stored energy in the liquid aluminum at the temperature of exothermic ignition, as measured with the differential thermal analysis, has been used as the measure of energy necessary to be transferred during impact to achieve ignition. Using the physical properties that 1 mole of aluminum weighs 26 grams, the density of aluminum is 2.7 grams/cm^3, 1 molar volume is approximately 10 cm^3, and the aluminum coating

thickness is 1 mm, the critical impact (combustion) area was calculated to be 16.9 cm² for the 700 Kg.·m drop and 3.8 cm² for the 144 Kg·m drop of the rusted steel onto aluminum (24-27). The calculated values are seen in Table 6. With this oxide (Fe_2O_3) scale of the steel drop specimen, the critical area is calculated to be 14 cm² for 700 Kg·m specimen and 3.4 cm² for the 144 Kg·m specimen. The ignition will occur if the impact area is less than these calculated critical areas, as illustrated in Figure 5.

Table 6. The calculated critical maximum impact areas.

Combination	ΔH_T(0.1mole) 0.1X10cm^2=1cm^3 (cal)	Impact Energy (144 Kg•m) in (cal)	Impact Energy 7000 J (700 Kg•m) in (cal)	Combustion area(cm^2) with 0.1 cm Thickness Δl	
				144 Kg•m	700 Kg•m
Al-Fe_2O_3 Literature	1024.5	337	1473	3.35	14
Al-Fe_2O_3	1005.3	337	1473	3.35	14
Al-wet rust	948.4	337	1473	3.55	15.5
Al-dry rust	872.5	337	1473	3.86	16.9

5.3.4. Spallation of Liquid Aluminum Particles during Impact

If, on impact, a location on the aluminum achieves sufficient energy to melt, and/or plastically deformed, partially melted aluminum in the form of small size particles will be ejected (spalling) (28). Figure 6 illustrates this aluminum spalling. Most likely some of the ejected particles will have sizes small enough for ignition (13, 19-21). Calculations, which are extremely dependent on the initial boundary conditions, can be made to report the amount of specific energy of interaction necessary to cause spallation during impact of the steel on an aluminum surface. The heat content of aluminum at its melting temperature (6890 cal/mole) is used as the threshold for spalling. The calculation requires knowledge of the weight and height of the steel over the aluminum and, most importantly, the dimensions of the aluminum that takes the impact. The following assumptions were made for this particular calculation. The aluminum is assumed to be a coating, which is 1mm thick. Two different energies of impact are considered, 144 Kg., which is similar to the Japanese and Korean tests, and 700 Kg·m, which is similar to the DNV tests. Then the contact area is calculated based on the assumption that all the impact energy converts into localized thermal energy resulting in no, or extremely local, plastic deformation. Figure 7 illustrates the results. The 700 Kg·m drop case requires a contact area of less than 21.4 cm². The 144 Kg·m drop case requires less than 4.9 cm². Because of the density of steel, the falling steel component will probably have a larger contact area than the calculated critical area based on energy transfer. If it were less than this critical area, the steel would most likely penetrate the aluminum and transfer most of the energy into plastic deformation, resulting in insufficient energy to melt and spall. It is also apparent that spallation and reaction with the atmosphere is more likely than straight thermite reaction because the melting temperature is significantly less than that of a

thermitic reaction and will be reached first and more often. Also, the critical area for spallation is greater than the critical area for a straight thermitic reaction.

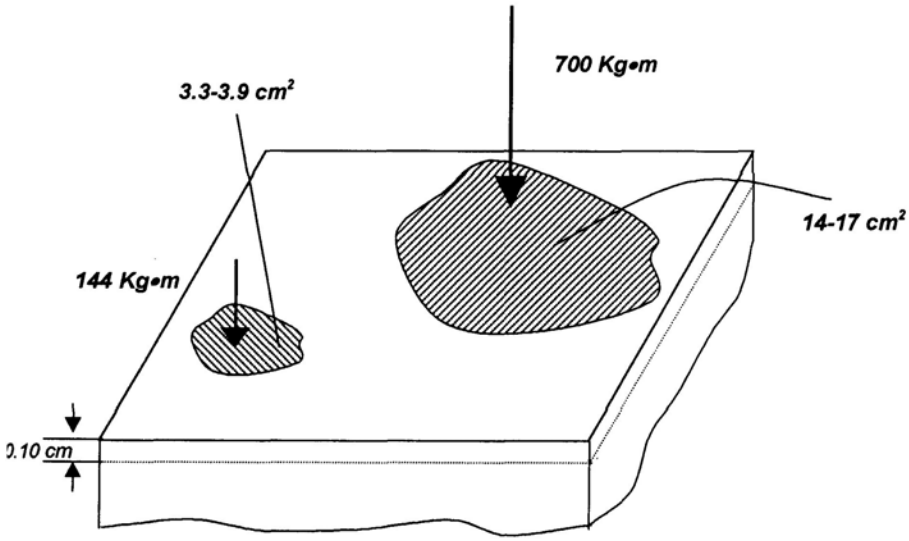

Figure 5. The critical contact areas for two different impact energies for comparison to the actual area on impact. If the contact area is less than this critical value, a thermite reaction is possible.

(a) 144 kg.m → contact area needs to be 3.3. – 3.9 cm^2 or less to react thermically (Japanese and Korean tests).

(a) 700 kg.m → contact area needs to be 14. – 17 cm^2 or less to react thermically (Norwegian tests).

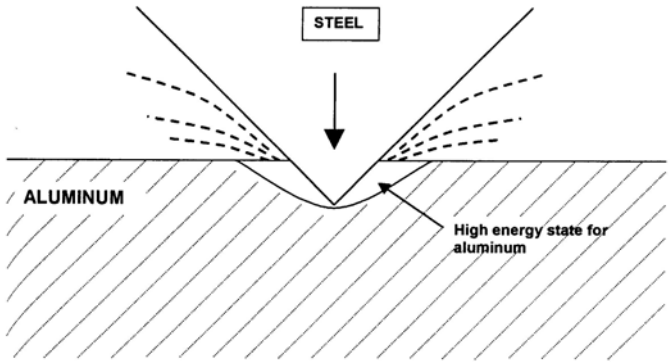

Figure 6. Aluminum Spalling During Impact of Steel into Aluminum

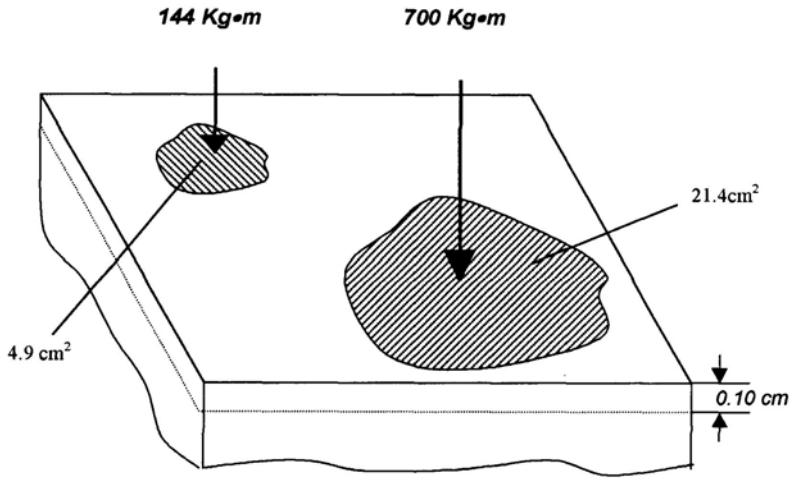

Figure 7. The critical areas of two different impact energies for comparison to the actual contact area on impact. If the contact area is less than this critical value, aluminum spalling can occur. The energy state of aluminum above the melting temperature at 660 ^{o}C (933 K) is 6890 cal/mole. The aluminum coating thickness of 0.1 cm was used in this calculation.

5.3.5. Hydrogen Generation Due to Wet Thermite Mixture

There was some reporting that wet industrial thermite mixtures have a problem with hydrogen generation during the thermite reaction. The hydrogen, if collected, has been reported to explode (23). The amount of hydrogen that would be generated during the time of impact is very unlikely to cause a microexplosion. There was no significant DTA exothermic peak suggesting a hydrogen reaction event.

5.4. Summary of Results of the Thermodynamic Evaluation

The literature search found that aluminum and iron oxide mixtures will react to produce a thermite reaction, but only after the temperature of approximately 1100ºC is reached (23). Also, it is apparent that extremely fine aluminum powder will react in air at room temperature. These observations raise the primary question as to whether the impact area can reach the high-energy state (1100ºC) to cause a thermite reaction or reach the melting temperature of aluminum (663ºC) to cause a spalling of fine aluminum particles, which can ignite in air.

Thermodynamic calculations of the heats of reaction for the various aluminum-oxide and aluminum-rust reactions were performed. Three oxides of iron and two rust types were included in these calculations. All combinations produced an exothermic reaction with the heat /mole of aluminum oxide ranging from -167 to -212 kilocalories/mole of aluminum oxide produced. The largest heat generation comes from

the oxide-aluminum mixture and the use of a rust reagent produces a smaller amount of heat, -167 kilocalories/ moles of aluminum oxide.

Differential thermal analyses of aluminum powder in mixtures of various oxygen sources (wet rust, dry rust and iron oxides) were performed. The reaction of the aluminum–oxide mixtures verified the literature reported results that thermite reactions require a temperature of approximately 1100ºC to ignite. This high temperature is achieved in thermite welding by the burning of a magnesium foil strip, which is embedded into the thermite mixture. The results for aluminum-dry rust showed the reaction required a lower temperature to ignite; approximately 970ºC is needed. The aluminum- wet rust mixture spent its energy on the endothermic release of water vapor.

The energy state required for aluminum to partake in the thermite reaction was determined with thermodynamic data and knowledge of the reported necessary temperature for thermite ignition. With this energy and knowledge of the impact energies, the maximum size of the impact area that can achieve sufficient localized energy to cause a thermite reaction was calculated for the aluminum mixture with dry rust and iron oxide. This calculation assumes the worst case of no plastic deformation during impact and a direct hit with no reflection. These calculated maximum impact areas were compared to and rationalized with the geometry of the falling weight. Qualitatively these comparisons suggest that it would be difficult to achieve the right impact configuration of the falling weight relative to the plate to result in a sufficiently small impact area to concentrate the necessary energy.

The necessary energy state for aluminum to enter into the liquid state was also acquired from the thermodynamic data. When the impact area achieved this energy there would be an expulsion of plastically deformed, partially melted aluminum particles. From the literature it is known that there is a critical size below which aluminum particles will ignite in air. These calculations suggest that the conditions for spalling would be more easily met in comparison to thermite reactions and, thus, represent the more probable mechanism for sparking. Considering the sizes of calculated maximum impact areas and remembering that these calculations assumed that all the energy is absorbed at this localized impact spot, spalling is not very likely to occur. There is also no evidence of sparking when aluminum is ground, due to its ability to plastically deform and transfer to other materials.

6. PHASE 2: IMPACT TESTING BETWEEN RUSTED/CLEAN PROJECTILE AND AL-COATED STEEL TARGET

Thermodynamic evaluation undertaken in this project may not entirely represent the actual impact incident between rust and Al-coated steel. The differential thermal analysis was done at a slow heating rate for accurate measurement of the ignition temperature and identification of the exothermic reaction. Such a slow heating condition, however, only corresponded to a near equilibrium reaction between rust and aluminum. On the other hand, impact incident between rust and aluminum, such as hammer falling down to the body of the tanker, is most likely to be extremely dynamic. To get a more convincing conclusion on the potential of sparking between rust and Al-coated steel, either by spallation or by thermite reaction, an experimental program was undertaken to create various impact incidences between the two materials of interest.

6.1. Experimental Apparatus and Procedures

The impact testing apparatus was designed and constructed based on the configuration shown in Figure 8. The apparatus, which resembles a rifle barrel, was powered by compressed gas to allow the impact / kinetic energy of the projectile to be varied over wide range of values. It was necessary to use a quick-opening solenoid valve (max thirty milli-second) just behind the projectile to enable quick triggering, so that the projectile felt the entire set pressure before being pushed out of the rifle barrel. In most cases, the rifle barrel was positioned with an approximately 0.2 meter distance between the end of the barrel and the target, except for the preliminary part of the investigation involving a 0.5 gram size projectile. Rigidity of the target mounting to the apparatus structure strongly affected the potential of sparking. The experiment was carried out after first ensuring that the target was firmly mounted on the apparatus structure.

Detection and recording of the spark was done by using a photodiode, also tailor-made for this experimental task. This photodiode generated an electric potential which, after being magnified by an operating amplifier, recorded the event with a strip chart reader. The output of the photodiode was unfortunately not linearly proportional to the light intensity of the source, in this case the spark. As demonstrated by two images of sparks shown in Figure 9, a dim spark was read as 0.5 mV while a very bright spark, appears to be ten times higher in intensity, was only read as 0.9 mV. Besides the intrinsic performance of the photodiode, the direction of sparks with respect to the location of the photodiode also influenced the outcome of the light intensity quantification. The images of the sparks were obtained by video recording, which was then followed by conversion to digital images.

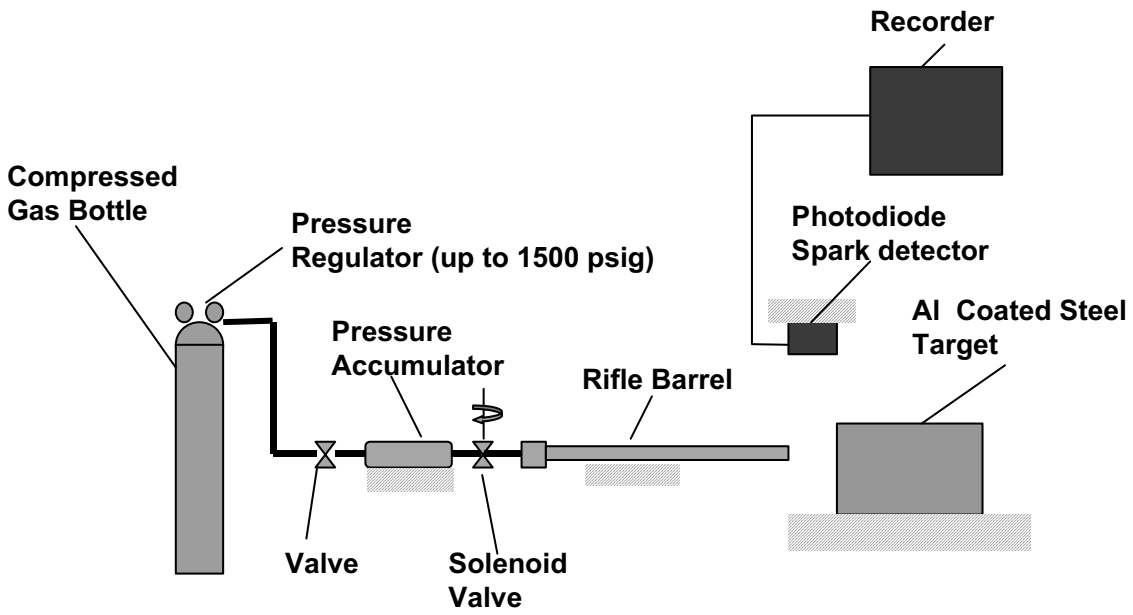

Figure 8. Configuration of the impact testing apparatus for observation of sparking between rusted steel and Al-coated steel.

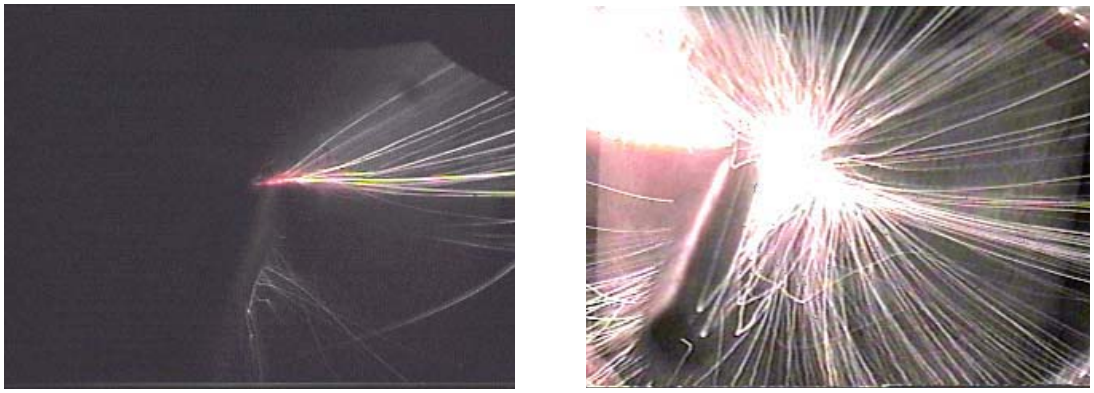

(a) (b)

Figure 9. Comparison of the spark images and the photodiode outputs for two different sparks (a.) 0.5 mV (b) 0.9 mV.

6.2. Preliminary Investigation of Impact Study

The decision to select the rifle barrel configuration for the impact testing was originally based on the thermodynamic evaluation in Phase I, which suggested that sparking would not easily occur during the impact incident. It was assumed that high impact velocity would be necessary to prove that there is a potential for sparking because the activation energy needed to ignite sparking needs must be high. The initial apparatus arrangement was constructed from a modification of a commercial air rifle. Hence, the projectile size is limited to the rifle barrel diameter, which was 0.177 inch (4.5 mm). To guarantee impact between rust and aluminum, the projectile was made by spot-weld joining two air rifle (spheres) bullets, followed by grinding one end of the projectile for the location of the rust. The impact surface after this grinding was approximately 0.08 cm^2 or 8 mm^2. The projectile, as heavy as 0.5 gram, is shown schematically in Figure 10, while its photographic documentation is included in Appendix A.

The lower range of velocity of this bullet was later measured by high-speed camera to be higher than 400 m/s. Hence, it was the impossible to measure the higher range of the bullet velocity with the available high speed camera used for this study. Impact energy was then measured by a simple pendulum configuration, which is schematically shown in Figure 11. A piece of wood was placed on the target surface of the pendulum to completely stop the incoming projectile. The impact energy for various set pressures of the rifle power source (compressed gas) is shown in Figure 12.

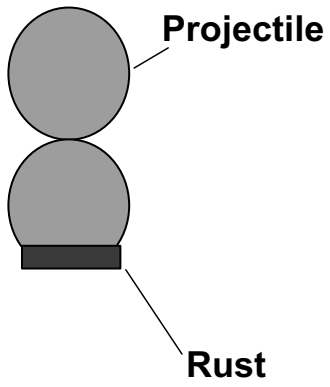

Figure 10. Configuration of the 0.5 gram projectile made for the preliminary impact testing.

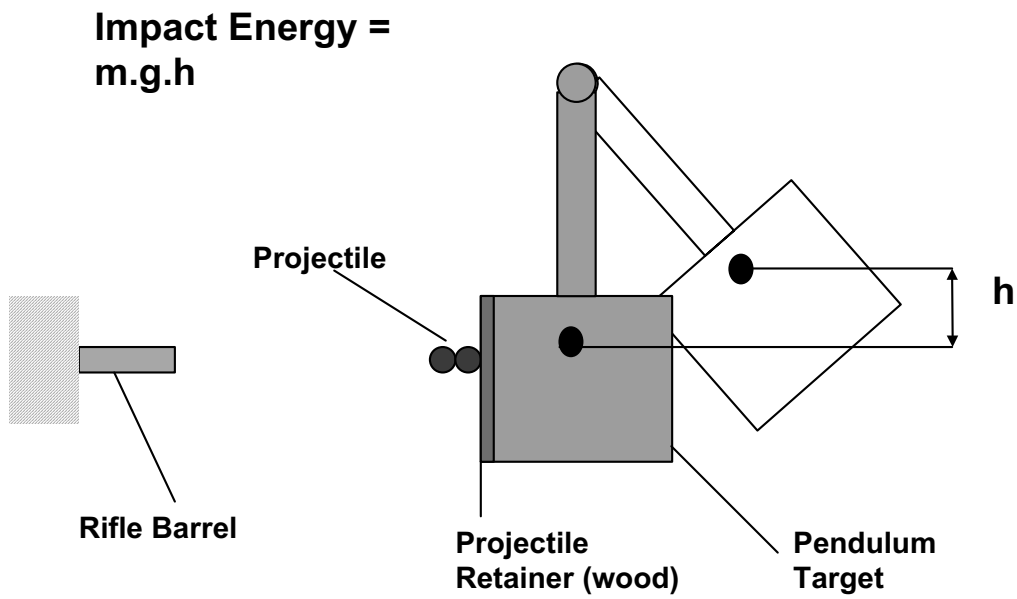

Figure 11. Pendulum set-up to measure the impact/kinetic energy of projectile.

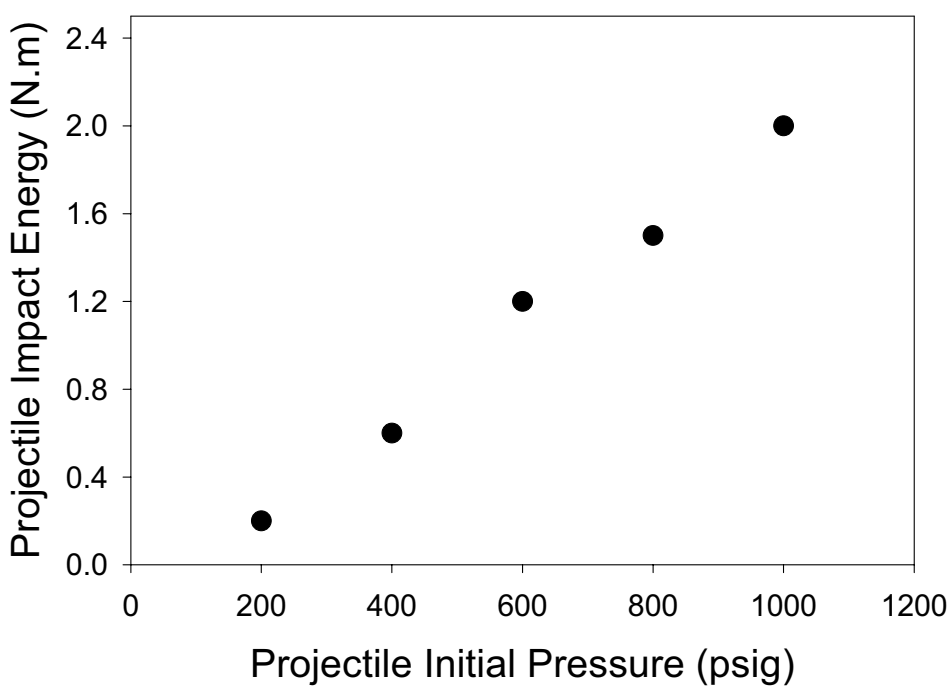

Figure 12. Impact / Kinetic Energy of 0.5 gram projectile as a function of set pressure.

The spark intensity of impact is shown in Figure 13. This figure shows the spark intensity of two different impact incidents: the first is between a rusted steel projectile and an Al-coated steel target, while the second is between a clean steel projectile and an Al-coated steel target. A threshold set pressure for ignition of spark was found to occur at a set pressure of 800 psig, both for rusted and clean steel projectiles. The clean steel projectile surprisingly generated small sparks at a set pressure higher than 800 psig. This set pressure corresponded to an impact energy of 2 Joule. With the known surface area of the projectile, which was 0.08 cm^2, the threshold impact energy density was calculated to be approximately 25 Joule/cm^2 or 2.5 kgf.m/cm^2. This value was much smaller than the threshold value as predicted by the thermodynamic evaluation (360-400 Joule/cm^2 or 36-40 kgf/cm^2). The thermodynamic prediction was calculated for a relatively thick aluminum coat, which is 0.1 cm. The coating thickness was measured to be in the order of 250 μm (0.025cm). In this case, the predicted threshold value for 250 μm thickness would be 90-100 Joule/cm^2, which is about four times as high as the measured value. It is possible that the amount of aluminum involved in sparking is much smaller than the volume covered by the whole impact surface area.

Impact beyond 800 psig set pressure generated intense sparking between rusted steel and aluminum. It should be noted that all the impact tests were performed on an excessive amount of rust with respect to the available amount of aluminum at the impact surface. On the other hand, the increase in spark intensity at higher set pressure than 800 psig was very small for clean steel projectiles. The presence of rust was obviously responsible for the amplification of spark intensity observed for the impact incidents involving rusted steel projectiles. Hence, thermite reaction might occur during this preliminary impact testing.

The mechanism of sparking for clean steel projectiles at such high impact energies was thought to be caused by spallation of the aluminum. As illustrated in Figure 14, initial contact between the flat-surfaced projectile and the curved-surfaced target was a very small area that may promote a very localized and rapid shearing of a small volume of aluminum, especially with the high impact velocity involved in this preliminary test. This high strain-rate deformation, without any chance of relaxation, would likely melt the small volume of aluminum under the impact load. The melted aluminum was possibly spattered away from the impact surface before a complete stop of the projectile. Complete stop of the projectile was then followed by macroscopic deformation of both the projectile and the target, which was observed in most cases. Localized melting of the aluminum coat was also thought to be necessary condition to ignite the thermite reaction between rusted steel and aluminum. Surface irregularities, either on the projectile or on the target (especially the steel substrate) would enhance this suggested spallation mechanism. Such a mechanism would also explain the smaller value of threshold impact energy than the thermodynamically predicted one. It was also possible that such spallation was a precursor to the thermite reaction observed on the case of impact incidents of the rusted projectiles, which is analogous to the differential thermal analysis where the aluminum had to melt before exothermically reacting with rust.

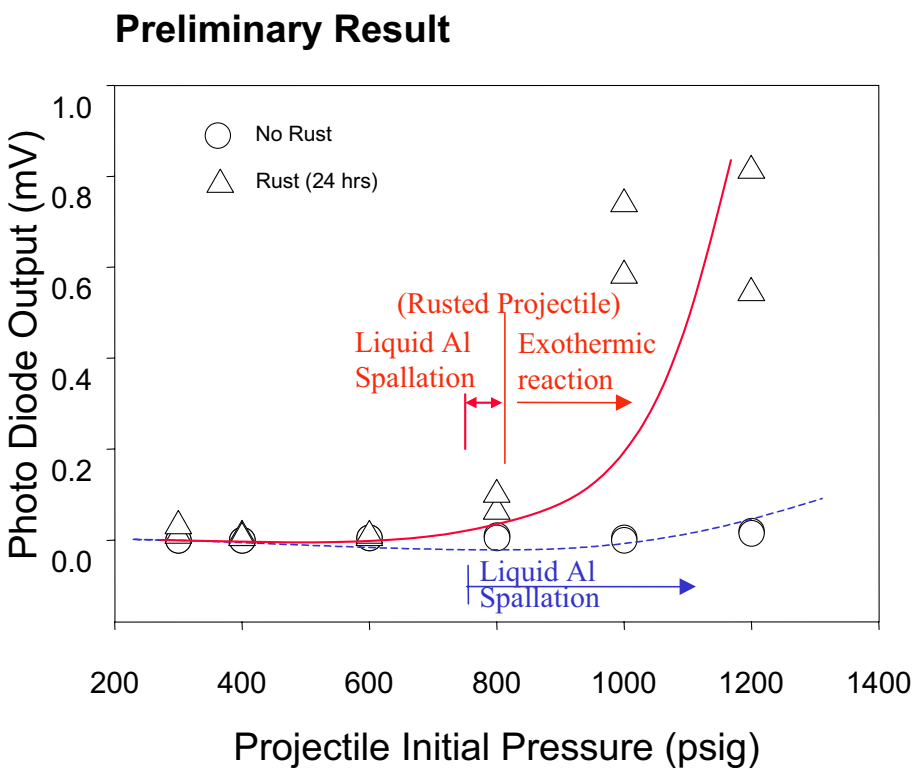

Figure 13. Spark Intensity for 0.5 gram projectile as a function of set pressure.

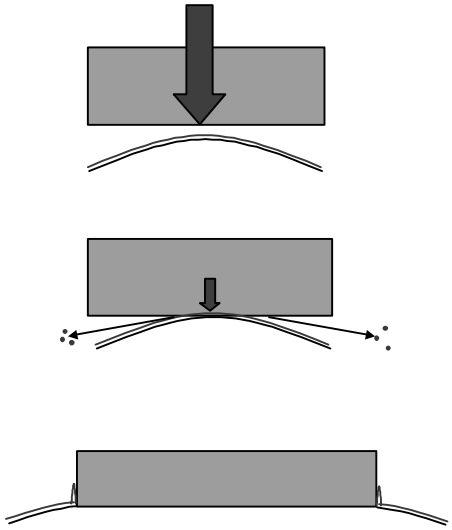

Projectile approaches
The Al-coated steel target

Projectile very locally deforms a very small volume of aluminum up to the thickness of the coating.
The localized deformation, as well as shearing, melted the aluminum and produced spallation/exothermic reaction

Macroscopic deformation of the projectile as well as the target

Figure 14. Possible mechanism of spallation aluminum from the Al-coated steel during an impact incident.

Preliminary investigation of the impact surface was performed using scanning electron microscopy. Figure 15.a. shows the impact surface as a result of collision between rusted steel and Al-coated steel when the rifle power pressure was set to 1000 psig (with spark occuring). Small pores can be easily noticed, which indicates some degree of gas pick-up, most probably by melted aluminum. Whether the melting occurred before or right after the high intensity sparking (presumably due to the thermite reaction) may need to be further investigated. If aluminum melting, which was then followed by spallation, indeed occurred before the sparking, then coating design may reduce this spark potential through careful consideration of the aluminum coating thickness and composition.

Even though this preliminary result has shown the potential for sparking upon the collision between rusted steel and Al-coated steel, the range of velocity used in this initial study was much higher than one would expect to see in any real impact incident most likely to be encountered with falling objects onto tanker and floating structures. One real example would be a hammer falling from the highest point down to the inner bottom of the tanker or floating structure. The velocity involved in these cases will be in the order of 10 to 20 m/s, for a dense and solid object falling down a distance between 5 to 20 meters. In contrast, this preliminary impact testing apparatus shot the projectiles at velocities higher than 400 m/s. The main activity of this experimental study should then be based on a test matrix involving a more practical range of impact velocities, as well as projectile masses.

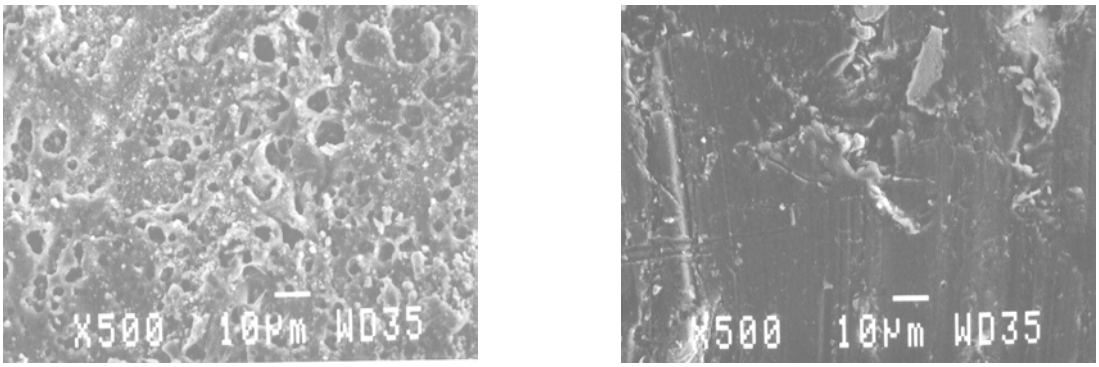

(a) (b).

Figure 15. (a) Impact surface of collision between rusted steel projectile (0.5 gr.) and Al-coated steel target at set pressure of 1000 psig. (b). as received Al-coated steel surface.

6.3. Main Investigation of Impact Study

This part of the experimental study addressed two main issues:

a. Whether an impact incident will generate sparks if the combination of velocity and mass of the projectile more closely approaches the values commonly encountered in real safety cases.
b. Whether the impact between rusted steel and Al-coated steel is any more susceptible to sparking than the impact between rusted steel and steel.

To respond to the first issue, a test matrix was programmed according to the values of projectile mass and rifle power set pressure as listed in Table 7. There were three variations of projectile mass: 25, 50, and 75 grams. These projectiles were made from steel rounds with a diameter of 0.5 inches (12.5 mm). To shoot these projectiles, a new rifle barrel with an appropriate barrel size was manufactured. To maintain the same impact surface area as that of the preliminary investigation, a smaller diameter pin (0.125 inch or 4.5 mm diameter) was anchored to the main projectile body, as shown in Figure 16. As with the 0.5 gram projectile used in the preliminary study, an excessive amount of rust was mounted on the tip of the projectile pin. Photographic documentation of these projectiles is also included in Appendix B.

The impact / kinetic energy of the three projectiles as a function of compressed gas set pressure was deduced from the velocity measurement of the projectiles with a high speed camera. A camera capable of recording images up to 6000 frames per minute was used, as shown in Figure A9 in the Appendix A. For high speed video recording, this camera requires a sufficient amount of illumination to be given to the moving object, disallowing the use of this equipment for spark recording in dark backgrounds. The velocities of the three projectiles for different set pressures are shown in Figure 17. The maximum projectile velocity used in this matrix was around 80 m/s, while the minimum one was 6 m/s. In these figures and others, the compressed gas set pressure unit is presented in psig, instead of in SI units. The reason is that this set pressure served only as a control value of the apparatus, not as direct measure of the energy given to the projectile. The impact / kinetic energy given to the projectile was calculated based on the measured velocity, as shown in Figure 18. Impact energy values of the 50 and 75 gram projectiles were practically identical. One value of set pressure of the apparatus apparently provided a fixed value of kinetic energy for the projectiles. The smallest projectiles, 25 gram, had lower values of impact energies, probably because the air friction consumed a good portion of its kinetic energies. The higher mass of the larger projectiles may have compensated for the loss of kinetic energies due to air friction.

Table 7. Test Matrix of the main experimental program

Projectile Mass	Projectile Tip Material	Target Material	Set Pressure
25 grams	dry rusted steel	Al-coated steel	25 – 1200 psig
50 grams	dry rusted steel	Al-coated steel	25 – 1200 psig
75 grams	dry rusted steel	Al-coated steel	25 – 1400 psig
75 grams	dry rusted steel	unprotected steel	25 – 1400 psig
75 grams	dry rusted steel damped rusted steel wet rusted steel	Al-coated steel	200 psig
75 grams	dry rusted steel damped rusted steel wet rusted steel	unprotected steel	200 psig

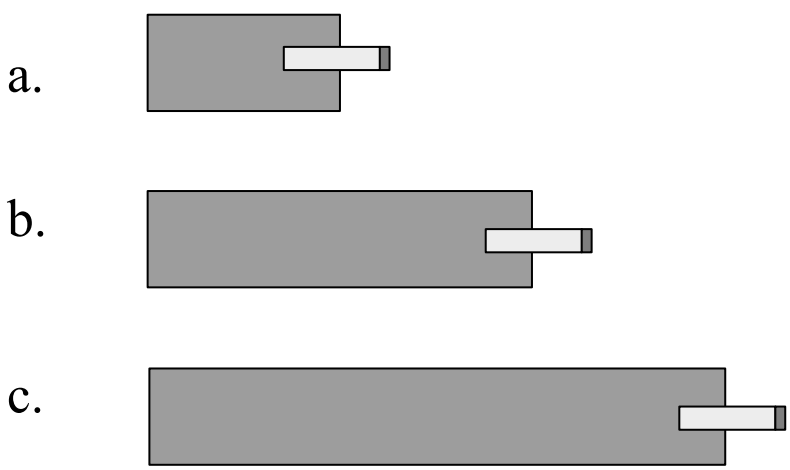

Figure 16. Configuration of the projectiles used for the main experimental program.(a). 25 grams: 0.5 inch ϕ × 1 inch (12.7 mm ϕ × 25.4mm) (b). 50 grams: 0.5 inch ϕ × 2 inches (12.7 mm ϕ × 50.8 mm) (c). 75 gram: 0.5 inch ϕ × 3 inches (12.7 mm ϕ × 76.2 mm)

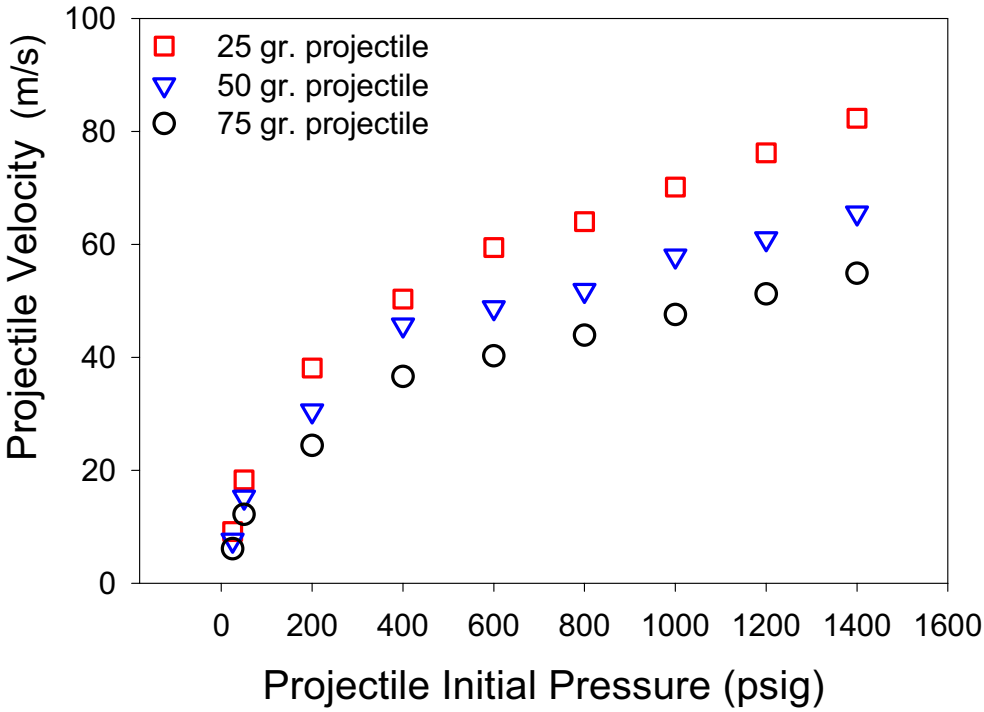

Figure 17. Velocity of the projectiles as a function of set pressure.

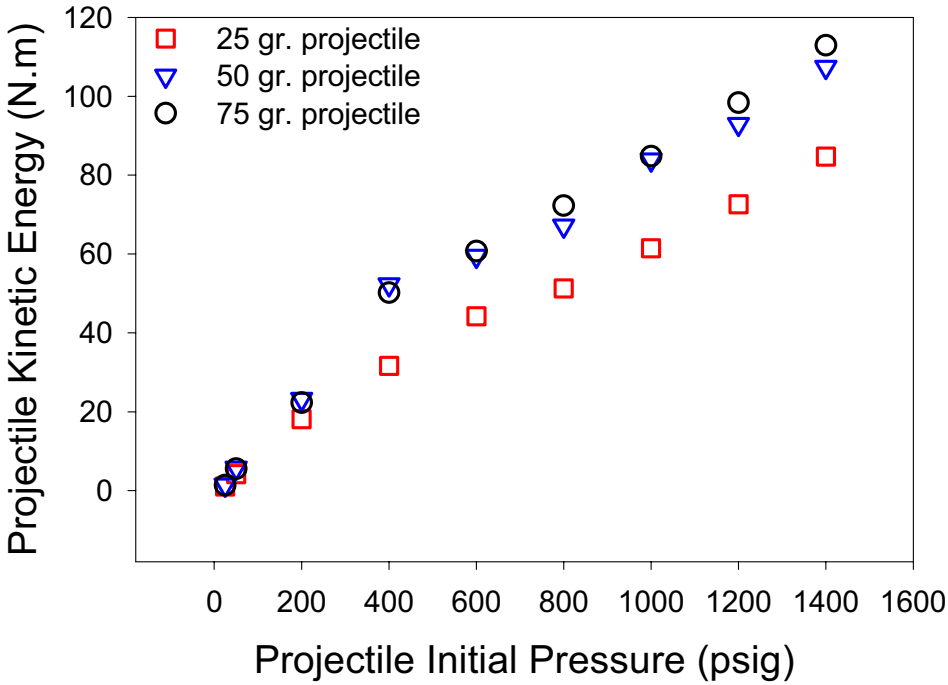

Figure 18. Impact/kinetic energy of the projectiles as a function of set pressure.

6.4. Results of the Main Impact Study

The experimental results are shown in Figures 19 to 21, for the 25 to 75 gram projectiles respectively. No clear pattern can be seen from the three figures, except that the probability for intensive sparking is high (above 75 percent) within set pressure values of 50 and 200 psig, as well as those values beyond 1000 psig. Between 200 and 1000 psig set pressure, the sparks had roughly a 50 percent chance of success. This result suggest that sparking might not occur at, for example, 800 psig set pressure even though the projectile possessed a kinetic energy much higher than a projectile shot with a set pressure of 50 psig. The causes for this behavior are not clearly understood. It is possible that the mechanism for sparking at the low set pressure regime is entirely different from that of the high pressure regime.

The set pressure of 50 psig is important not only because is it the apparent threshold value for spark ignition, but it also produced very high spark intensities. Unlike the threshold sparking previously observed for the 0.5 gram projectiles in the preliminary study, this later threshold sparking will need serious attention in conjunction with the fire hazard potential it may present. The set pressure of 50 psig, as shown in Figure 17, produced projectile velocities between 10 and 20 m/s, a range of values that fall within the focus of attention for safety concerns. It also is worth mentioning that impact incidents for the three sizes of projectile at a set pressure of 25 psig, which corresponded to projectile velocities of 5 to 7 m/s, did not ignite sparks.

Selected spark images accompanying the three figures are presented to illustrate the contrast of spark morphology between the various values of set pressure. The individual spark images, along with other selected ones, are presented in more detail in Appendix C. The sparks resulting from high impact energies appeared to be continuous and flame-like. Even though this morphology resembles a combustion reaction, this image may also be produced by very finely distributed droplets of liquid aluminum, traveling at a very high velocity. In contrast, individual droplets of liquid aluminum can be clearly seen in sparking images resulting from low set pressure. It was also noticed that the spatter velocity of sparks (perhaps aluminum droplets) at low value of set pressure was much slower than that produced by high set pressure. This low spatter velocity might give more time for photodiode detection, which in turn gave an output quantity as high as or even higher than those values of sparks produced by high set pressure.

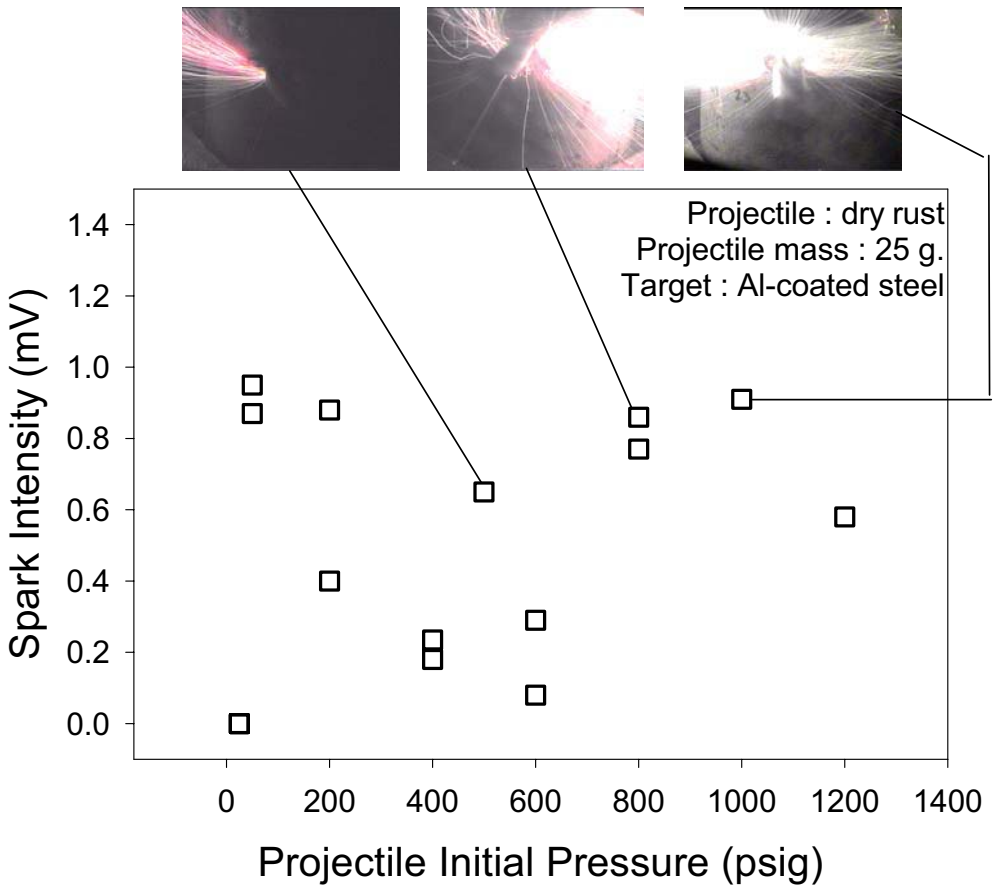

Figure 19. Spark Intensities of impact incident of 25 gram rusted steel (dry) projectiles with Al-coated steel target, as a function of set pressure.

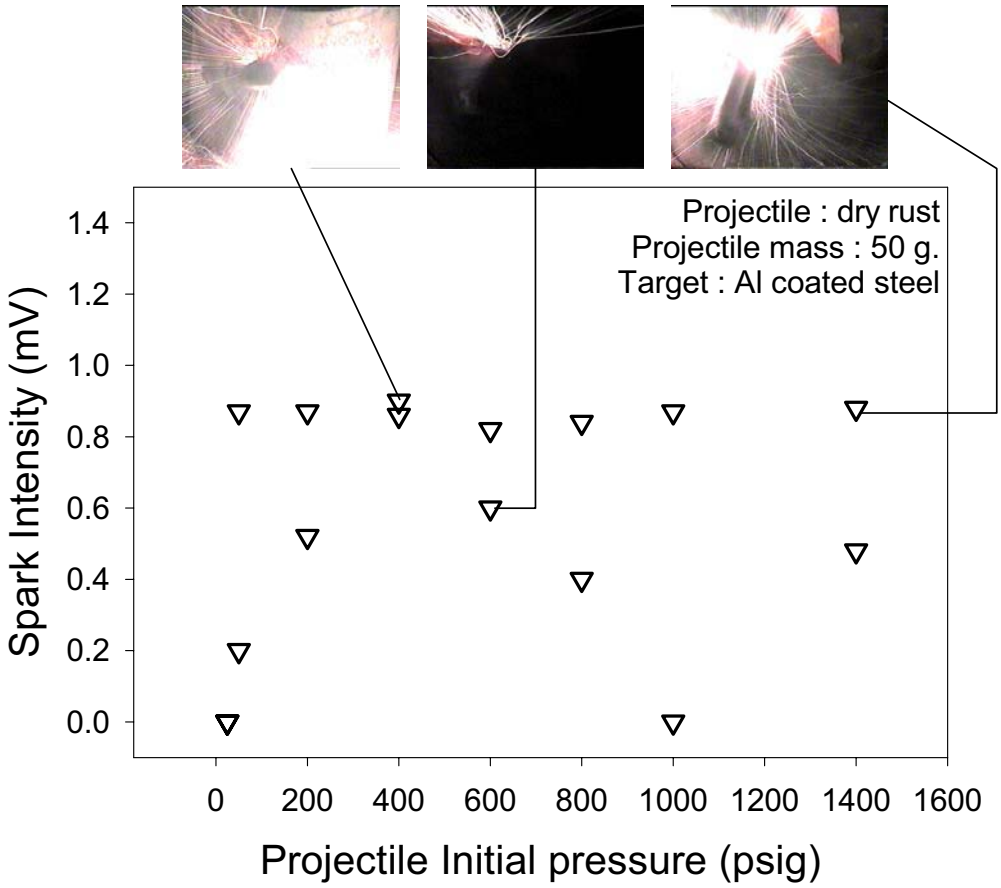

Figure 20. Spark Intensities of impact incident of 50 gram rusted steel (dry) projectiles with Al-coated steel target, as a function of set pressure.

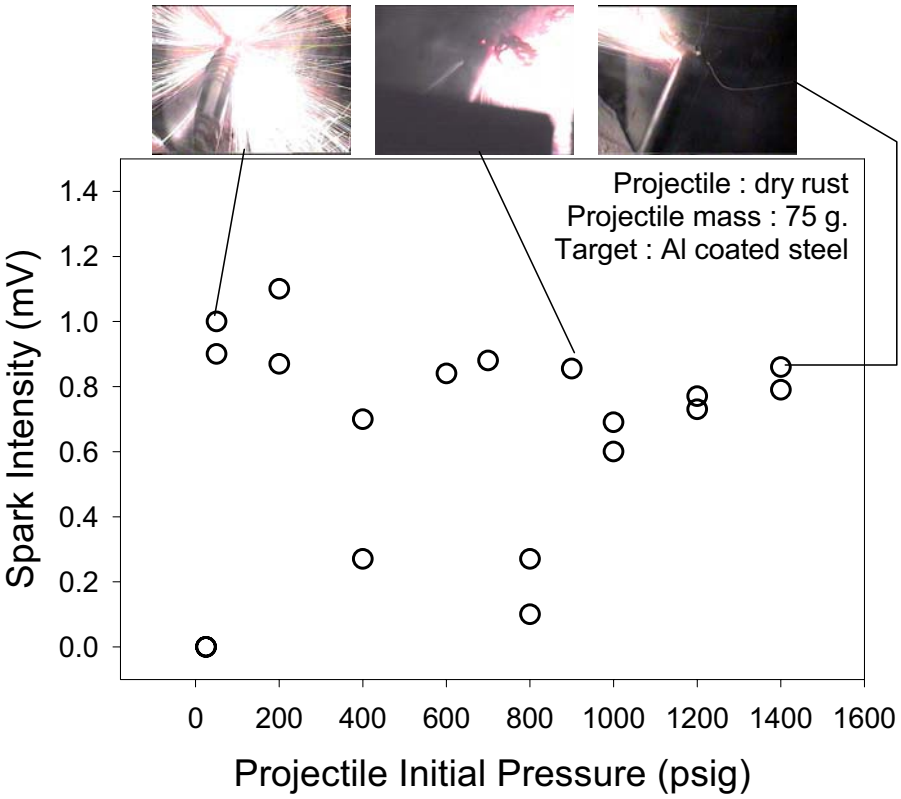

Figure 21. Spark Intensities of impact incident of 75 gram rusted steel (dry) projectiles with Al-coated steel target, as a function of set pressure.

As a response regarding impact between rusted steel and steel, which was addressed in this study, a series of rusted projectiles were shot to hit a clean steel target. This test was done only for the 75 gram projectile and its result is shown in Figure 22. This figure clearly shows that sparks were ignited even without the presence of aluminum. The threshold pressure for this incident was 100 psig, which corresponded to a projectile velocity of 20 m/s. Spark intensity increased as the set pressure was increased up to 400 psig, then diminished again beyond 600 psig. This result shows that it is possible to ignite a spark upon an impact incident between rusted steel and clean steel, with friction between rust and steel as the plausible mechanism to intensively increase the temperature of the impact surface. Also, the low thermal conductivity of the rust might have caused a very localized heating of the impact surface during the impact. One would question whether the sparking at low velocities was controlled by the rust itself rather than the rust interaction with the target material. It would then be of scientific interest to investigate the impact incident of rust with other hard target materials. Even though sparks occurred without the presence of aluminum coat, it is still too early to suggest that aluminum coat does not present a greater potential to fire threat. In fact, the aluminum coat on the steel target has been clearly shown to enhance the sparking susceptibility of this rust, both by lowering the threshold impact energy and by increasing the spark intensity.

To investigate the contribution of aluminum spallation to spark ignition, impact incidents between clean steel projectiles and Al-coated steel targets were generated using only the 75 gram projectiles. The result is shown in Figure 23. As shown, no sparks were observed at any value of set pressure. Spallation did not appear to contribute to the ignition of sparking in low regimes of projectile velocities. This result implies that spallation requires an adiabatic heating of a very small volume of aluminum coat, such as the heating that occurred in the preliminary study with very high velocities of projectiles (higher than 400 m/s). However, it is still possible that the presence of rust on the tip of the projectile caused a very localized friction and shearing of aluminum to occur due to the surface irregularities of the rust. Such a localized energy dissipation might cause partial melting of aluminum, even though not followed by spattering.

Finally, the effect of water content in the rust was investigated on the 75 grams projectiles. A constant set pressure of 200 psig was selected for this investigation. The result, shown in Figure 24, highlighted the role of aluminum coat on steel in stabilizing or enhancing the ignition of spark, especially with regard to a damped rust condition.

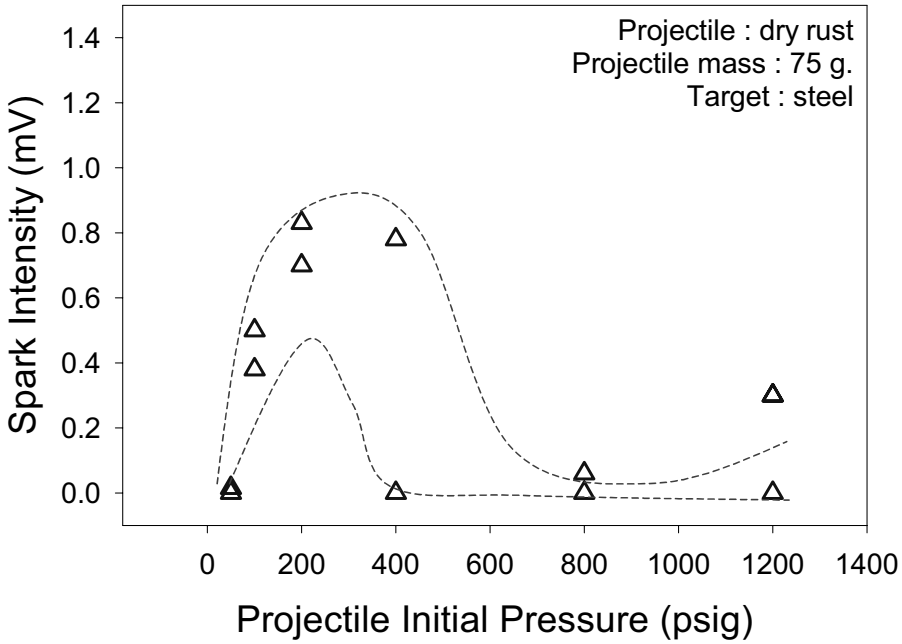

Figure 22. Spark Intensities of impact incident of 75 gram rusted steel (dry) projectiles with steel target, as a function of set pressure.

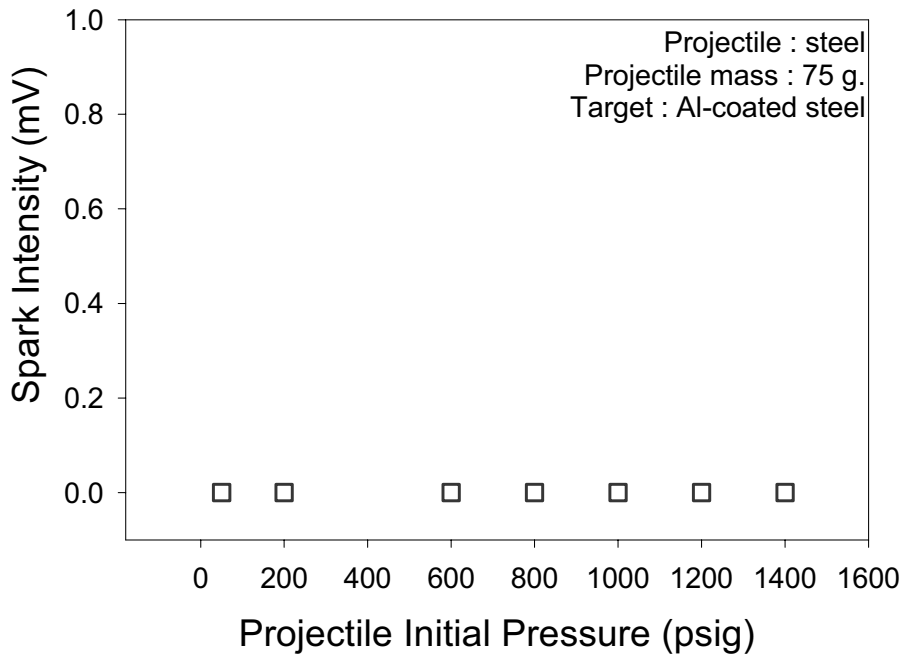

Figure 23. Spark Intensities of impact incident of 75 gram clean steel projectiles with Al-coated steel target, as a function of set pressure.

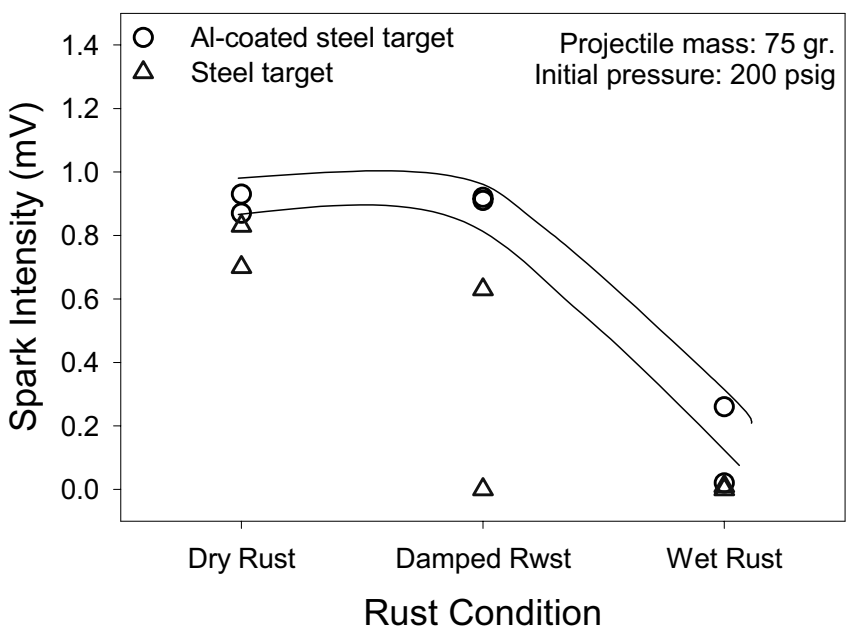

Figure 24. Spark intensity of impact incident of 75 gram rusted projectiles shot with set pressure of 200 psig and with various water content in the rust.

6.5. Discussion of the Impact Study

As mentioned in the results section, no clear pattern of sparking tendencies can be observed from the impact testing of the three projectiles, particularly when the spark intensities are plotted against the set pressure. The whole set of data for the three projectiles is plotted again in Figure 25. The data appears to be scattered randomly, with only one conclusion that can be drawn from it: the threshold sparking occurred at a set pressure of 50 psig. This threshold impact incident corresponded to an impact/kinetic energy of 4 to 6 Joule, or energy density of 50 to 75 Joule/cm^2 (calculated for the projectile 0.125 inch or 4.5 mm diameter tip area). Similar to the discussion mentioned in the preliminary study, this energy density is smaller than the thermodynamic prediction, which is 90-100 Joule/cm^2 (assuming the thickness of the aluminum coat is 250 μm). The same argument may still hold to explain these sparks, that the contact surface upon initial collision (before the complete stop of the projectile) involved an area much smaller than the diameter of the tip of the projectile.

A better pattern of data was observed when the whole data was plotted against the velocity of the projectiles, as shown in Figure 26. In this figure, one can see that high spark intensity was highly probable for either low or high projectile velocities. The probability for sparking at the medium regime of projectile velocities (40 to 60 m/s) appeared to be limited by fifty percent. It is too early to suggest that such an anomaly is real; more data is needed to allow for a better interpretation. However, such information, supported by a more careful study of the sparking mechanism, may need to be done in the future to help improve the design of aluminum coating on steel. The influence of aluminum alloy content and coating thickness are parameters which can potentially reduce or alleviate the sparking behavior.

As summarized in Figure 27, for 75 gram projectiles, both unprotected and Al-coated steel target accommodated sparking when hit by rusted steel (dry) projectiles. The rust itself may intrinsically have its own potential to ignite sparking when given sufficient activation energy. The cause of this spark ignition is still not understood. It should be remembered that rust is a primary source of oxygen. It is also apparent that rust has the capability to adiabatically convert the impact energy to heat, which will be readily available for immediate use of any kind of exothermic reaction between chemical species contained in the impact enclave. However, such an argument fails to explain the observed drop of sparking intensities with increasing impact velocity (above 30 m/s in Figure 27). On the other hand, the aluminum coating was indeed responsible for the threshold impact velocity observed at 12 m/s, which is lower than the velocity of 20 m/s for rusted steel impact onto steel without aluminum coating. In addition, it is of great concern that the spark intensity at this 12 m/s threshold impact velocity is remarkably high.

Unlike in the preliminary study, the investigators cannot suggest that aluminum spallation preceded the thermite reaction at this threshold impact incident. The consistently zero spark intensity observed for steel projectiles colliding onto Al-coated steel at various impact velocities clearly indicated that no spallation occurred for the combination of mass and velocity used in the main experimental study. However, this lack of sparking did not necessarily mean that there was no localized melting of aluminum on the impact surface.

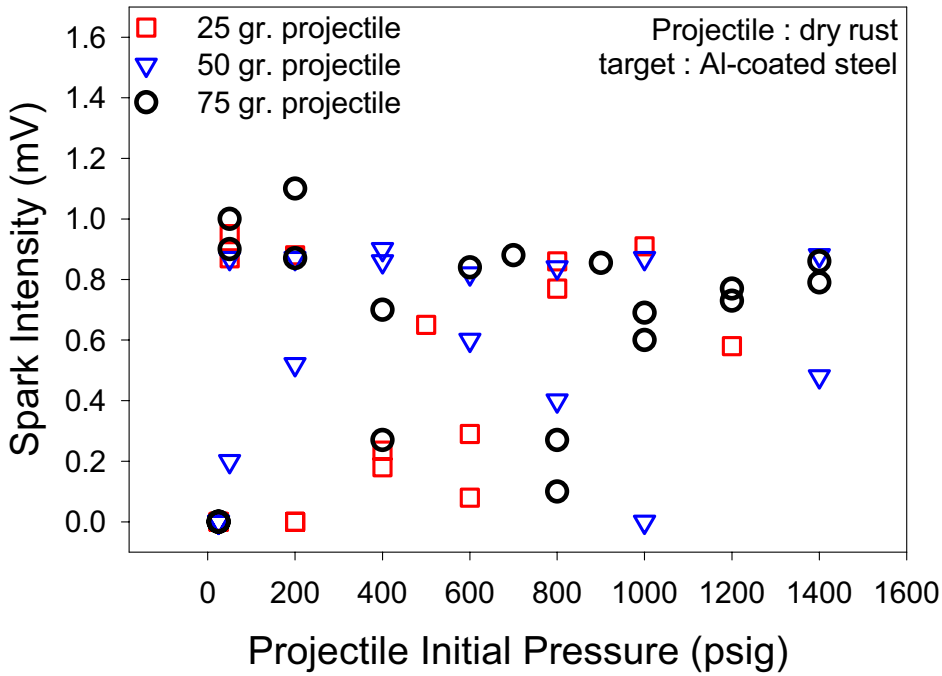

Figure 25. Spark intensities of three projectiles upon impact incidents involving rusted steel (dry) and Al-coated steel, as a function of set pressure.

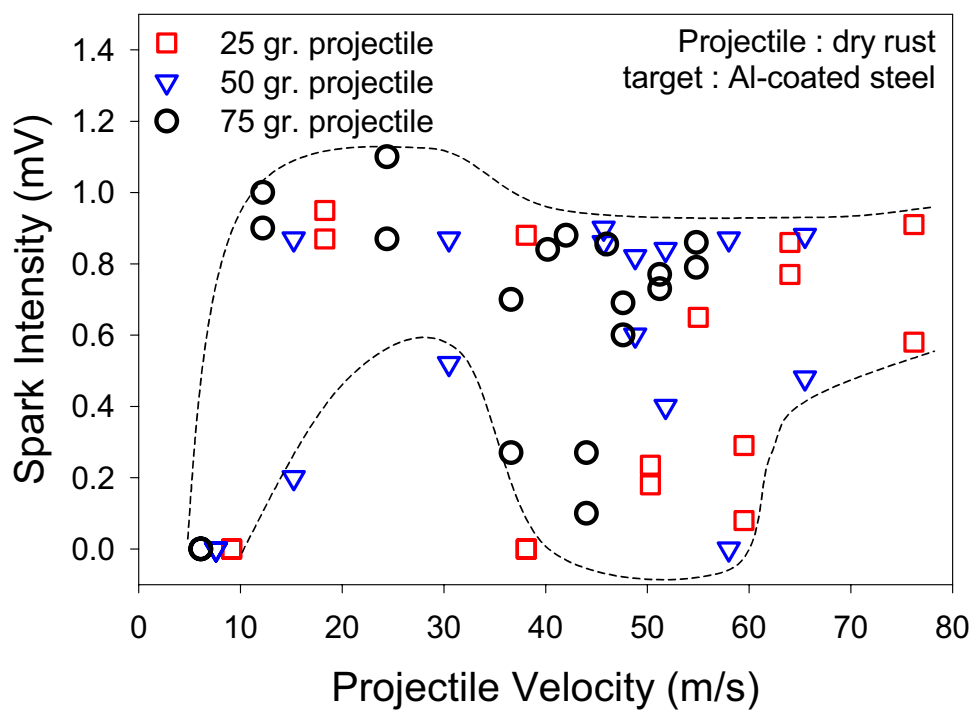

Figure 26. Spark intensities of three projectiles upon impact incidents involving rusted steel (dry) and Al-coated steel, as a function of impact velocity.

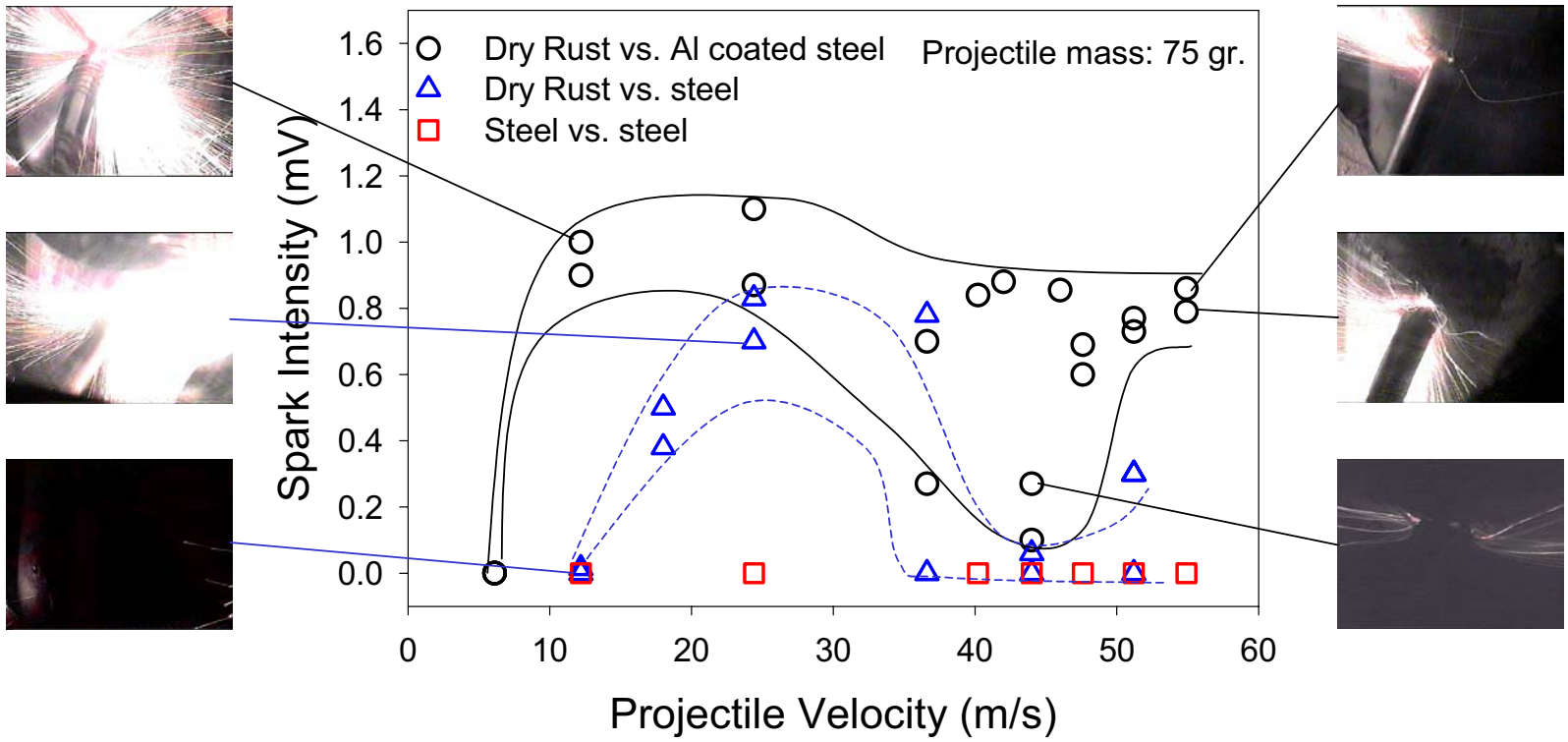

Figure 27. Summary plot of spark intensities as a function of projectile velocity for different type of projectiles.

Although the above details will need further investigation, the technological merit of this study is quite clear. The presence of aluminum enhances the sparking susceptibility upon an impact incident between rusted steel and Al-coated steel. However, this enhancement, which implicates aluminum coating as an additional fire threat to tankers and floating structures, is not excessive. Only at low impact velocities is aluminum more of a fire threat than uncoated steel. Above 20 m/s impact velocity, there is no difference between the two cases as to their potential for fire threat. Improvement in the metallurgical design of the aluminum coating, including the coating thickness, processing methods, as well as alloying design, may alleviate this aluminum fire threat to a level identical to that of the uncoated steel.

It should be noted that the photographic image of the sparks did not completely illustrate the real different of spark behavior between low and high velocity impact incidents. Direct observation of the video recording reveals that spatter velocity of particles during low velocity impact was also slow, allowing more time for photodiode detecting and, in turn, giving a deceiving impression that the spark intensity was as high as that which occurred during the high velocity impact. A relevant issue to be addressed then is whether the spark temperature of the low velocity impact is high enough to ignite a combustion reaction of air-natural gas mix.

6.6. Summary of the Impact Study

The following conclusions can be drawn from the experimental study:

1. The mechanism of sparking between rust and aluminum upon impact incident is complex. Investigation of the impact surface revealed some evidence of partial melting of aluminum whenever sparking occurred. This finding is consistent with the differential thermal analysis that necessitated the melting of aluminum prior to the ignition of exothermic reaction between rust and aluminum.

2. At higher impact velocity, it is clear than spallation, as a consequence of aluminum melting, precedes the exothermic reaction between rust and aluminum. On the other hand, low velocity impacts were found to be free from spallation of aluminum melts.

3. Dry rusted steel is intrinsically a potential fire threat due to its sparking potential during an impact incident with steel. To generate sparks, rust must convert the impact energy adiabatically into heat, which is then used to any potential exothermic reaction of chemical species trapped within the impact enclave. The threshold impact velocity for this sparking was found to be approximately 20 m/s for 75 gram projectiles. This impact incident would be identical to a 75 gram object falling down a 20 meter distance.

4. Aluminum coating on steel is found to be a slightly higher potential fire threat than un-coated steel during impact incidents with rusted steel. The threshold impact velocity for sparking between a rusted projectile and Al-coated steel was 12 m/s for 75 gram projectiles. This impact incident would be identical to a 75 gram object falling down an 8 meter distance. It is possible that partial melting of aluminum, at very localized

regions on the impact surface, accelerated the exothermic reaction between rust and aluminum. It is anticipated that improvement in the aluminum coating design would alleviate its fire hazard potential.

5. Water content on rust was found to reduce susceptibility to sparking in both Al-coated and uncoated steels. However, when the rusted steel projectile was wet, Al-coated steel was found to be more spark susceptible than uncoated steel at an equal impact velocity. In the extremely wet environment, un-coated steel did not generate sparks while Al-coated steel could still generate a spark, even though of small to moderate intensity.

7. PHASE 3: COMBUSTION TESTING UPON IMPACT BETWEEN RUSTED PROJECTILE AND Al-COATED STEEL TARGET

The potential for fire hazard upon impact between rusted projectile and Al-coated steel target was further evaluated with a combustion test of the successful spark incidents. This test was necessary for the completeness of this investigation to verify that the spark incidents will initiate combustion. The possibility that not every condition favorable for sparking will ignite combustion can be easily demonstrated. In a small experiment, involving steel grinding in front of feeding propane-fueled brazing torch, continuous spark generation during grinding did not initiate combustion in an optimum air-propane mixture. Combustion occurs if the combination of spark temperature / intensity and the air-flammable gas mixture is proper. Therefore, in the following experimental tasks, the combustion of different air-flammable gas mixtures, to be ignited by the spark incident of interest, was systematically investigated.

7.1. Experimental Apparatus and Procedures

Considerable efforts have been put forth in redesigning and upgrading the stationary compressed gas-powered impact apparatus due to fire safety regulation that has to be complied by the Colorado School of Mines. Essentially, the reconstruction involved parts feeding combustible gas and air into the impact chamber. The mixture of air and combustible gas is to be varied systematically to allow for the identification of a threshold mixture for combustion reaction. Several upgrading tasks were completed prior to combustion tests:

1. Transportation of apparatus for field study

The combustion study should not be done in an enclosed room in order to prevent fire hazard in the building due to accumulation of un-ignited combustible gas. To allow for easy transport in and out of the building, the structure was expanded from the original frame size (constructed for the previous phase of the study, as shown in Figure 28). Heavy-duty rollers were used to safely carry the compressed gas bottles along with the experimental set-up structure.

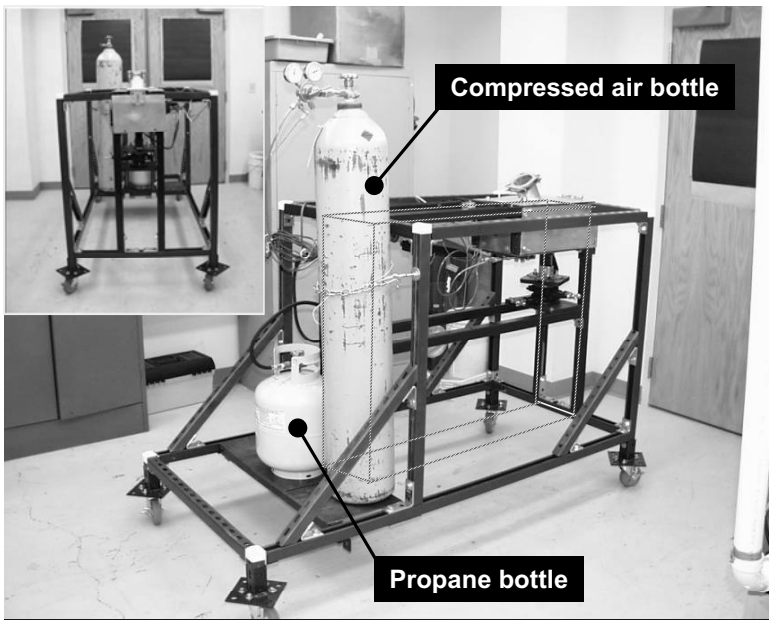

Figure 28. Side view of the expanded structure of the experimental apparatus, equipped with heavy-duty roller for enhanced mobility.

2. Air and combustible gas feeding

A mixture of air and combustible gas will be fed into the chamber where impact between rusted projectiles and aluminum-coated steel occurs. Therefore, this chamber is now also the combustion chamber. Figure 29 highlights the air and the combustible gas supply lines that ultimately feed into an acetylene torch. The use of the acetylene torch has made it easy to attain a variable ratio of air to combustible gas mix. Figure 29 also shows the projectile launching system (already constructed in the previous phase of the study).

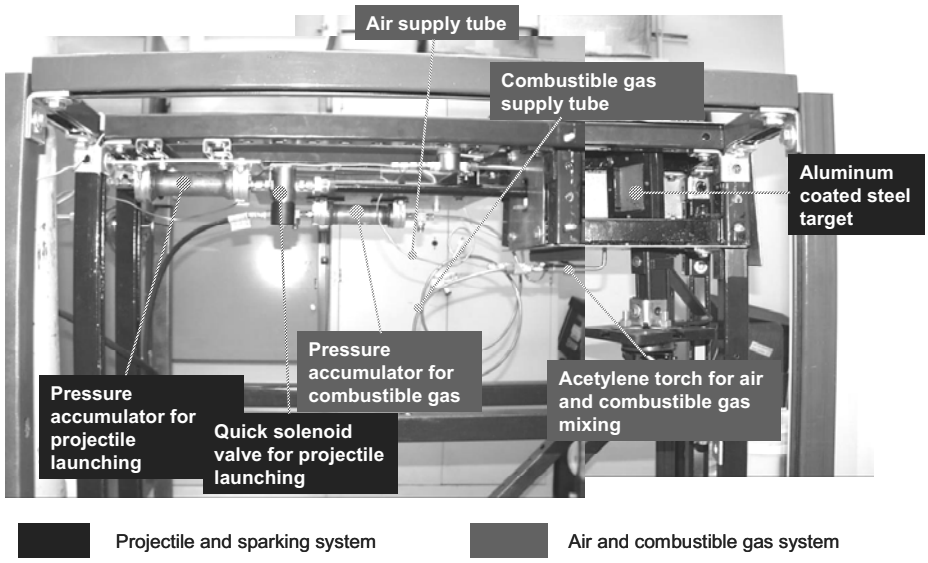

Figure 29. Detailed side view of the expanded structure of the experimental apparatus, with the air and combustible gas feeding lines being highlighted. Both air and the combustible gas are fed into an acetylene gas torch before the torch is placed into the combustion chamber. Also shown are the projectile compressed gas launching system and the target fixture (inside the combustion chamber).

3. Projectile velocity measurement by a chronograph

Even though the previous phase has involved accurate measurement of velocities of the various projectiles by a high-speed camera, reliable results in the following phases would continue to require assessment of this velocity. To enable field operation, a chronograph was installed on the experimental set-up to replace the need for a high-speed camera. Figure 30 shows the particular parts associated with the chronographs. Two light sensitive detectors were attached to the impact / combustion chamber to record the starting and ending time of the projectile on a length of projectile trajectory. From the time of travel, the velocity is calculated. A light source is also placed on top of the chamber for the light sensitive detectors to function properly. The slowest measurable velocity is 30 ft/s (10 m/s), which is slightly lower than the threshold velocity required for the 75-gram projectile to create sparking.

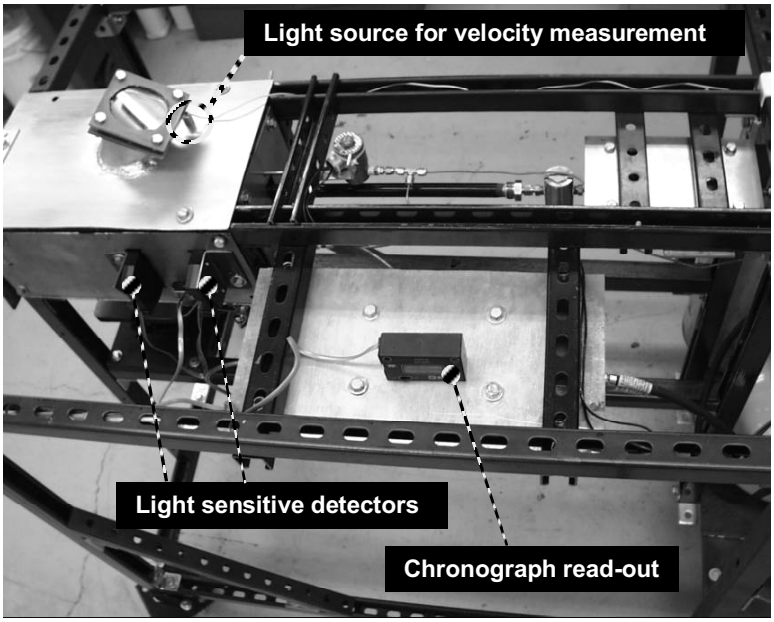

Figure 30. Top-left view of the expanded experimental apparatus, with highlights of the velocity measurement device (chronograph).

4. Modification of the fixture to hold the Al-coated steel plate target

When changing from pipe targets to plate targets, a new fixture was constructed. To allow for several impact spots occurring in one plate target, the fixture was made with a capability for X-Y position adjustment, as shown in Figure 31. Also shown in Figure 31, the fixture is capable of angular position adjustment, a variable that will also be investigated in this phase of study. The thin Al-coated steel plate is sandwiched between two 12.5 mm plate steel frames for sufficient rigidity. The front frame has a square hole for exposure of the aluminum surface, but the back frame is completely solid.

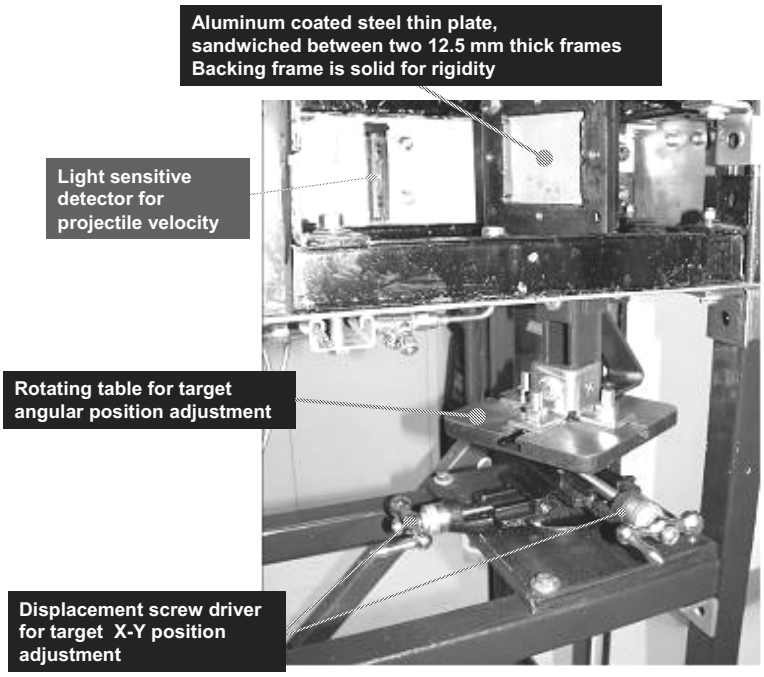

Figure 31. Side view of the fixture for the Al-coated steel target with X-Y and angular adjustment. The target thin plate is sandwiched between two 12.5 mm thick steel frames for increased rigidity.

5. Controlled mixing of air and combustible gas.

To precisely mix air and the combustible gas in a prescribed ratio, the corresponding gases are fed into a balloon. In this way, the gas mixture is securely contained to minimize possible sources of disturbance, particularly the effect of wind. The earlier practice was to feed air first and to measure the diameter of the balloon. Afterwards, the combustible gas is fed, followed by measurement of the final diameter of the balloon. With this practice, a rough estimate of the ratio between the two gases can be obtained. Figure 32 shows the gas-filled balloon inside the combustion chamber. Before launching the rusted projectile, the balloon will be punctured by a nail so that the balloon will not be squeezed in between the tip of the projectile and the impact target. The nail will be launched from a separate compressed-gas-powered tube, as also shown in Figure 32. A quick-opening solenoid valve is used for the launching of this nail, as shown in Figure 33.

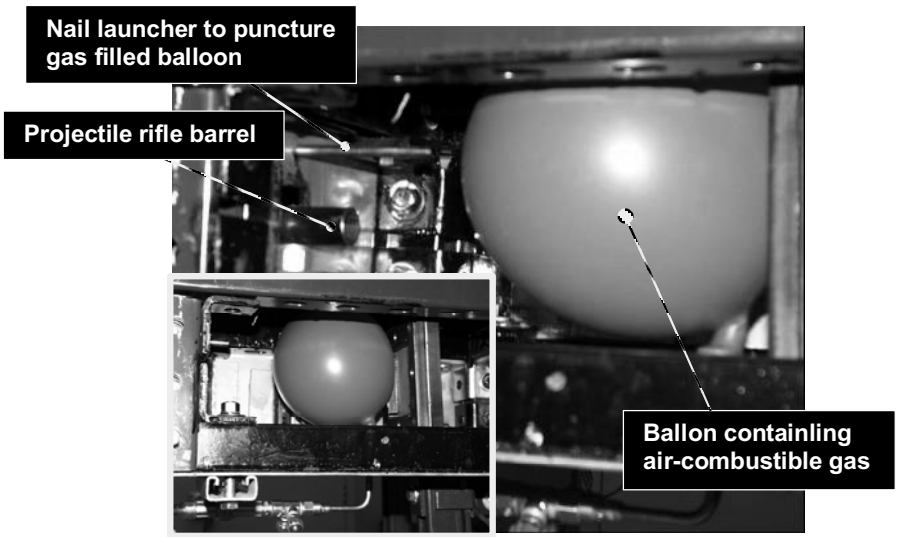

Figure 32. Side view of the combustion chamber with the gas filled balloon in front of the Al-coated steel target. Separate feeding of the gases (air and combustible gas) is anticipated to allow for a reasonable estimate of the ratio between the air and the combustible gas. Also shown are the projectile rifle barrel and the nail launching tube.

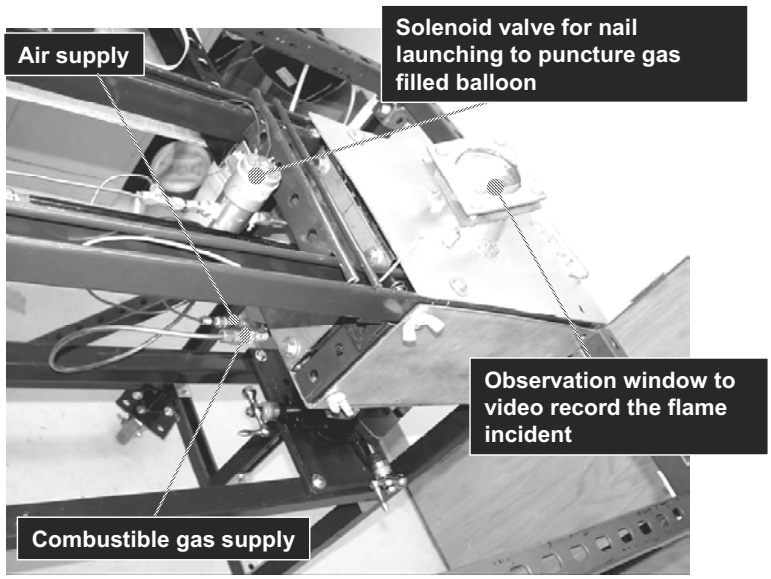

Figure 33. Top-right view of the expanded experimental apparatus, with highlights of the gas-filled balloon puncturing system (solenoid valve), and air-combustible gas feeding system, as well as the observation window for video recording purposes.

7.2. Experimental Design for Combustion Study

In this phase, sparking incidents with the same sizes of projectiles were generated with Al-coated steel plates, with approximately 250 μm thick aluminum coating (impact targets in phase 2 were pipes). The short-term objectives of this phase are:

- Identification of a threshold ratio of mixing of air and combustible gas required for a combustion reaction to occur at a particular impact or spark condition.
- Identification of a threshold impact or spark condition required for a combustion reaction to occur, at a constant mix of air and combustible gas.
- Observation of the effect of impact angle on the threshold values required for a combustion reaction.

To achieve these objectives, the experiment was designed with:

- Variations in Combustible Gas: mixture of air with methane, propane, acetylene, and gasoline vapor.
- Variations in Projectile Velocity: 10, 20, and 30 m/s.
- Variation in Impact Angle: 90 and 60 degrees.

Investigation in this phase focused on the projectile mass of 75 grams and velocity between 10 and 30 m/s. The selected impact was between dry rust and Al-coated steel, as has been shown in the previous phase to be the greatest potential spark generator. A specific ratio of air to gas was mixed inside a balloon, which was to be punctured about one second before the launching of the projectile. The reported air-flammable gas mixtures were not the actual mixture during the test. The actual mixture was lower than the reported values because there was some dilution of the mixture by additional air inside the test chamber, after the puncture of the combustible-mixture-containing balloon. Each air-gas mixture was verified for their combustion range with an electric igniter.

Unlike the flammable gas, gasoline was fed by wetting filter papers with the fuel. The filter papers were placed on the bottom floor of the chamber and on the target surface. Projectile was released after a few minutes from the gasoline feeding to allow enough vapor generation in the chamber. Flammability of the gasoline feed was also verified with the electric igniter. It was found that flame occurred as the spark of the igniter's electric wire touch the filter paper, rather than coming from the gasoline vapor.

7.3. Results on the Combustion Study

Tables 8 through 14 contain the results of the combustion experiments with the projectile trajectory perpendicular to the target surface. These results covered all the combinations of the flammable gas-air mixture and the projectile velocities. For these perpendicular impact incidents, each combination was repeated for four times of successful spark generation. About twice as many impact trials had to be conducted in acquiring these results because the probability of generating sparks during this phase of study was approximately 70 percent. It was not clear whether the rust condition or the precision of impact surface contact was the cause of this rather low probability for spark generation. Only the experimental observations with successful spark generations, which were clearly visible, were reported in the results of Tables 8 through 14. However, most of the combinations were found to be unsuitable for combustion with the observed

sparks, except for some of the rich mixture of acetylene and air (at an acetylene/air ratio higher than 0.25). On the other hand, all mixtures were verified as suitable to cause combustion with the electric igniter.

Tables 15 through 18 present the results from impacts, angled 60 degrees from the target surface. During this study, the success probability for sparking during impact experiments, with an angle between projectile trajectory and the target, was very low because the difficulty in the set-up. This very low probability is reflected in the higher number of unsuccessful spark generations in the corresponding tables. Proper orientation of the projectile with respect to the target surface was thought to be the crucial factor to get a successful spark generation. It was unfortunate that this factor was difficult to control during the experiment because, in reality, most sparking incidents involving falling objects will be in an angle with the target.

The results pertaining to the air-gasoline vapor mixture are presented in Tables 19 and 20. As in the case of flammable gas-air mixture, the sparks did not ignite any flame on the gasoline-wetted filter papers. The sparks were successfully generated, even though the rusted tip of the projectile had to impact through the filter papers that were placed on the target surface. Such a placement of the filter paper should ensure that the sparks were in the closest possible vicinity to the gasoline vapor during their highest intensity condition; hence, the life time of sparks should not be an issue. As a comparison, a small experiment involving steel grinding very close to a wetted filter paper did not ignite any flame either.

Table 8. Results from the combustion test, in air-propane mixture, upon the impact incident between rusted projectiles and Al-coated steel. Impact incidents were perpendicular with 10 m/s projectile velocity.

Test	Condition			Observation		
	gas	gas vol. fraction	Projectile Velocity	angle (degree)	spark	flame
1	propane				Yes	No
2		100			Yes	No
3					Yes	No
4					Yes	No
5					Yes	No
6		50			Yes	No
7					Yes	No
8			10 m/s	90	Yes	No
9					Yes	No
10		25			Yes	No
11					Yes	No
12					Yes	No
13					Yes	No
14		10			Yes	No
15					Yes	No
16					Yes	No

Table 9. Results from the combustion test, in air-propane mixture, upon the impact incident between rusted projectiles and Al-coated steel. Impact incidents were perpendicular with 20 m/s projectile velocity.

Test	Condition			Observation		
	gas	gas vol. fraction	Projectile Velocity	angle (degree)	spark	flame
17					Yes	No
18		100			Yes	No
19					Yes	No
20					Yes	No
21					Yes	No
22		50			Yes	No
23					Yes	No
24	propane		20 m/s	90	Yes	No
25					Yes	No
26		25			Yes	No
27					Yes	No
28					Yes	No
29					Yes	No
30		10			Yes	No
31					Yes	No
32					Yes	No

Table 10. Results from the combustion test, in air-propane mixture, upon the impact incident between rusted projectiles and Al-coated steel. Impact incidents were perpendicular with 30 m/s projectile velocity.

Test	Condition			Observation		
	gas	gas vol. fraction	Projectile Velocity	angle (degree)	spark	flame
33					Yes	No
34		100			Yes	No
35					Yes	No
36					Yes	No
37					Yes	No
38		50			Yes	No
39					Yes	No
40	propane		30 m/s	90	Yes	No
41					Yes	No
42		25			Yes	No
43					Yes	No
44					Yes	No
45					Yes	No
46		10			Yes	No
47					Yes	No
48					Yes	No

Table 11. Results from the combustion test, in air-methane mixture, upon the impact incident between rusted projectiles and Al-coated steel. Impact incidents were perpendicular with 10 m/s projectile velocity.

Test	Condition			Observation		
	gas	gas vol. fraction	Projectile Velocity	angle (degree)	spark	flame
49	methane	100	10 m/s	90	Yes	No
50					Yes	No
51					Yes	No
52					Yes	No
53		50			Yes	No
54					Yes	No
55					Yes	No
56					Yes	No
57		25			Yes	No
58					Yes	No
59					Yes	No
60					Yes	No
61		10			Yes	No
62					Yes	No
63					Yes	No
64					Yes	No

Table 12. Results from the combustion test, in air-methane mixture, upon the impact incident between rusted projectiles and Al-coated steel. Impact incidents were perpendicular with 20 m/s projectile velocity.

Test	Condition			Observation		
	gas	gas vol. fraction	Projectile Velocity	angle (degree)	spark	flame
65	methane	100	20 m/s	90	Yes	No
66					Yes	No
67					Yes	No
68					Yes	No
69		50			Yes	No
70					Yes	No
71					Yes	No
72					Yes	No
73		25			Yes	No
74					Yes	No
75					Yes	No
76					Yes	No
77		10			Yes	No
78					Yes	No
79					Yes	No
80					Yes	No

Table 13. Results from the combustion test, in air-methane mixture, upon the impact incident between rusted projectiles and Al-coated steel. Impact incidents were perpendicular with 30 m/s projectile velocity.

Test	Condition			Observation		
	gas	gas vol. fraction	Projectile Velocity	angle (degree)	spark	flame
81	methane	100	30 m/s	90	Yes	No
82					Yes	No
83					Yes	No
84					Yes	No
85		50			Yes	No
86					Yes	No
87					Yes	No
88					Yes	No
89		25			Yes	No
90					Yes	No
91					Yes	No
92					Yes	No
93		10			Yes	No
94					Yes	No
95					Yes	No
96					Yes	No

Table 14. Results from the combustion test, in air-acetylene mixture, upon the impact incident between rusted projectiles and Al-coated steel. Impact incidents were perpendicular with 10 m/s projectile velocity.

Test	Condition			Observation		
	gas	gas vol. fraction	Projectile Velocity	angle (degree)	spark	flame
97	acetylene	50	10 m/s	90	Yes	**YES**
98		25			Yes	No
99					Yes	Yes
100					Yes	No
101					Yes	No
102		10			Yes	No
103					Yes	No
104					Yes	No
105					Yes	No

Table 15. Results from the combustion test, in air-propane mixture, upon the impact incident between rusted projectiles and Al-coated steel. Impact incidents were 60 degrees angled with 10 m/s projectile velocity.

Test	Condition			Observation		
	gas	gas vol. fraction	Projectile Velocity	angle (degree)	spark	flame
106	propane		10 m/s	60	Yes	No
107		100			No	No
108					Yes	No
109					No	No
110		50			No	No
111					Yes	No
112					Yes	No
113		25			Yes	No
114					No	No

Table 16. Results from the combustion test, in air-propane mixture, upon the impact incident between rusted projectiles and Al-coated steel. Impact incidents were 60 degrees angled with 30 m/s projectile velocity.

Test	Condition			Observation		
	gas	gas vol. fraction	Projectile Velocity	angle (degree)	spark	flame
115	propane		30 m/s	60	No	No
116		100			No	No
117					Yes	No
118					No	No
119		50			No	No
120					No	No
121					Yes	No
122		25			Yes	No
123					No	No

Table 17. Results from the combustion test, in air-methane mixture, upon the impact incident between rusted projectiles and Al-coated steel. Impact incidents were 60 degrees angled with 10 m/s projectile velocity.

Test	Condition			Observation		
	gas	gas vol. fraction	Projectile Velocity	angle (degree)	spark	flame
115	methane	100	10 m/s	60	No	No
116					No	No
117					No	No
118		50			No	No
119					Yes	No
120					No	No
121		25			Yes	No
122					No	No
123					No	No

Table 18. Results from the combustion test, in air-propane mixture, upon the impact incident between rusted projectiles and Al-coated steel. Impact incidents were 60 degrees angled with 30 m/s projectile velocity.

Test	Condition			Observation		
	gas	gas vol. fraction	Projectile Velocity	angle (degree)	spark	flame
124	methane	100	30 m/s	60	Yes	No
125					No	No
126					Yes	No
127		50			No	No
128					Yes	No
129					No	No
130		25			Yes	No
131					No	No
132					No	No

Table 19. Results from the combustion test, in air-gasoline vapor, upon the impact incident between rusted projectiles and Al-coated steel. Impact incidents were perpendicular.

Test	Condition			Observation		
	Fuel		Projectile Velocity	angle (degree)	spark	flame
133	Gasoline				Yes	No
134			10 m/s		Yes	No
135					Yes	No
136					Yes	No
137					Yes	No
138			20 m/s	90	Yes	No
139					Yes	No
140					Yes	No
141					Yes	No
142			30 m/s		Yes	No
143					Yes	No
144					Yes	No

Table 20. Results from the combustion test, in air-gasoline vapor, upon the impact incident between rusted projectiles and Al-coated steel. Impact incidents were 60 degree angled.

Test	Condition			Observation		
	Fuel		Projectile Velocity	angle (degree)	spark	flame
133	Gasoline			60	No	No
134			10 m/s		Yes	No
135					No	No
136					Yes	No
137					Yes	No
138			20 m/s		No	No
139					No	No
140					Yes	No
141					No	No
142			30 m/s		No	No
143					Yes	No
144					No	No

7.4. Discussions and Verification Tests on the Combustion Study

As mentioned in the beginning of this section, small sparks from steel grinding did not ignite a flame out of a feeding propane-fueled brazing torch. This experiment demonstrated that not all sparks have the potential to ignite combustion. With the exception of the air-acetylene gas mixture (results in Table 14), it suggests that the spark condition, associated with the impact between rusted steel projectiles and the Al-coated steel, had a similar character with that generated during steel grinding. The small number of combustions observed for the air-acetylene mixtures might be caused more by the pressure sensitivity of the gas, than the condition of the sparks. High-pressure sensitivity of air-acetylene gas mixture is a well-known property.

The temperature of the sparks might be insufficient to cause ignition in the whole range of air-flammable gas mixtures used in this study. It is also worth mentioning that the whole range of air-flammable gas mixtures used was found combustible, either with the electric or flint igniter. The sparks generated by flint obviously had much higher intensity or temperature than those sparks generated from the impact incidents of interest. Therefore, the difference in spark temperatures between the two spark origins may be a major factor for ignition of the combustion. On the other hand, combustion ignition with electric sparks, which were essentially electrically-heated thin stainless steel wires, actually did not have an appreciably high intensity of light. Qualitatively, the intensity of these electric sparks was lower than these of the flint sparks. It was also occasionally observed that combustion with this spark took place with a longer incubation time. Unlike the impact sparks that travel very quickly, electric sparks were stationary. This observation suggests that, given sufficient time for heat exchange and reaction activation to take place, combustion could be ignited with relatively low temperature sparks.

The results obtained thus far raised some questions regarding the peculiarity of the experiment apparatus developed in this study, as compared to those set-ups used by other investigators. Combustions had been observed with the traditional drop test method, although the probability of such an event was quite low. This low probability might be caused by non-uniformity of the rust condition on the impacting surface, and spark generation during the drop test was not consistent. The large mass used in the drop test method (corresponding to a weight of at least 700 kgf.), accompanied by large area of the impact surface, had the potential to trap and increase the local pressure of air-flammable gas mixture, especially between the surface irregularities. Such an increase in pressure would enable ignition of the air-gas mixture at a low spark temperature associated with the impact between rusted projectile and Al-coated steel. The probability of having such a mechanism in the present experimental study would be very small.

Some additional tests were conducted to verify and explore some possibilities that may have caused the absence of combustion in this study. Two of the tests listed below have been mentioned earlier in this section. These tests were:

1. The current experimental set-up might create a condition unsuitable for ignition of combustion, mainly due to the way the projectile was launched with a compressed air power source. Upon triggering the quick opening valve up-stream to the projectile, rapid flow of air might have followed, or even flow in advance of the traveling projectile. Such a rapid flow of air, which occurred instantaneously, might have displaced the combustible air-gas mixture around the impact target area. Therefore, at

their most suitable condition to ignite combustion, the sparks traveled through a volume of air instead of the combustible mixture. However, it was verified that this possibility is not significant. In a small experiment with electric igniter, it was found that combustion occurred when the projectile was launched just immediately before the triggering of the electric igniter. In this verification experiment, the compressed air was set at a value corresponding to the projectile velocity of 30 m/s, the highest velocity in this phase of investigation. This pressure or velocity should represent the worst condition for combustion associated with dilution of the combustible mixture. The electric igniter was carefully installed to be right on the path of the projectile trajectory.

2. Secondary to the above limitation (dilution of combustible mixture), the amount of sparks generated by the impact incident might be too small to achieve a high probability for a traveling spark to meet a local air-gas mixture with the proper condition for combustion. Ignition of combustion may depend on the lifetime and the number (and distribution) of sparks, and high density of impact sparks may be critical to observe combustion. To evaluate this possibility, additional impact tests were carried out with a modified projectile to allow for a larger impact surface. The projectile, as shown in Figure 34, had side holes that merge into a main longitudinal hole that ends at the impact surface. These holes were made to allow air to flow within the projectile, in order to minimize dilution of combustible mixture in front of the projectile. The inside cavity provided by these holes also should serve to increase the density of impact sparks. However, initial tests of this projectile did not successfully generate sparks, even at the increased power air pressure needed to compensate for larger rust and Al-coated steel impact surface area. This finding gave an additional implication on the generation of sparks with the originally designed projectile. One should consider that perpendicular impact, which definitely occurred with this modified projectile (larger impact surface), might not be the right condition for spark generation. It was highly possible that, with the original projectile, the rust got rubbed or ground on the target surface during impact due to the buckling of the tip of the projectile, which carried the rust.

3. A small experiment was carried out to find out whether steel grinding in front of feeding propane-fueled brazing torch would ignite flame or combustion. No ignition of flame was observed during a prolonged feeding of the propane-air mixture in front of the sparks generated by steel grinding. The intensity of the sparks was qualitatively comparable to that of the sparks generated by the impact study, and lower than the intensity generated by flint (which was able to ignite the combustible mixture of interest by default). Figure 35 shows the spark intensity of such steel grinding. This observation had several implications:

   a. The temperature of the sparks was not high enough to ignite combustion.
   b. The surface character of the sparks did not catalyze the ignition of a spark.
   c. There was a incubation time needed to ignite flame such that traveling sparks, such those generated during impact or grinding, did not have sufficient time to be in contact with a local combustible mixture. This aspect may be associated with heat

transfer from spark to the combustible mixture, activation energy for combustion, and, again, the temperature of the sparks.

4. A parallel experiment to the one above was carried out to show that flame could be ignited upon propane feeding with the brazing torch in front of a hot alumina brick heated at 1200 C. Flame was indeed ignited by this glowing object. Figure 36 shows the intensity of the glow of the brick at the time of flame ignition. In this picture, which highlights the intensity of the glowing brick, the flame was not stable yet and its image was not clearly captured. Compared with Figure 35, the intensity of the glowing brick appeared quite comparable, considering that the conditions (background) for image capturing between the two figures were not identical. This observation supported the suggestion that the electric spark in the impact study ignited the combustion due to the combination of sufficient thermal mass and the fixed location of the electric sparks.

5. Another experiment was carried out to determine whether steel grinding in front of gasoline-wet filter paper would ignite flame or combustion. As with the previous trial, no ignition of flame was observed, even though the sparks touched the wet paper while still at their high intensive condition. As during the impact study, the sparks did not seem to preferentially ignite the gasoline vapor-air mixture. It is worth mentioning that the gasoline-wet filter paper can cause flame ignition upon contact with flint sparks.

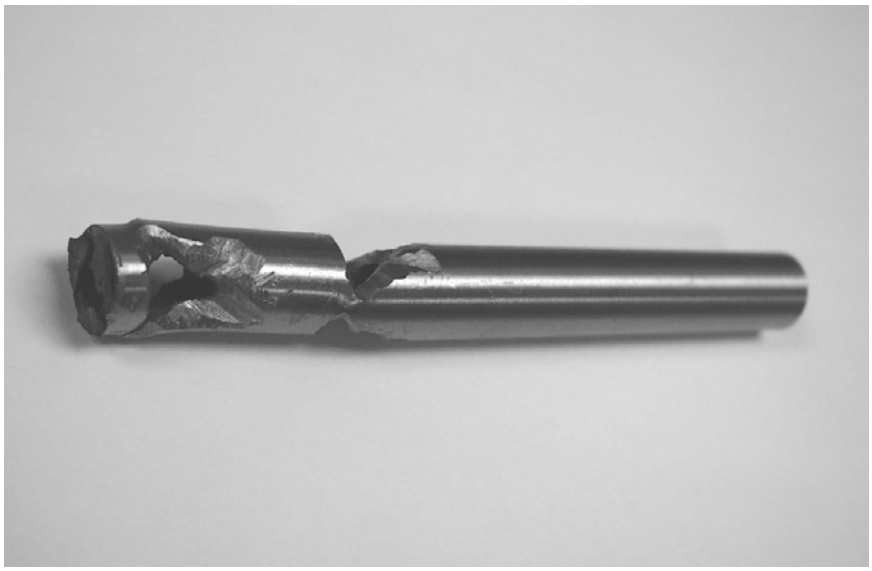

Figure 34. Modified projectile carrying larger amount of rust on the left end. Starting from this end, a main longitudinal hole penetrates more than half of the length of the projectile. Four side holes, which merge into the main longitudinal hole, were made to allow air to flow through the projectile as it launched for the impact.

Figure 35. Sparks generated by steel grinding, which did not ignite flame for the propane-fueled brazing torch.

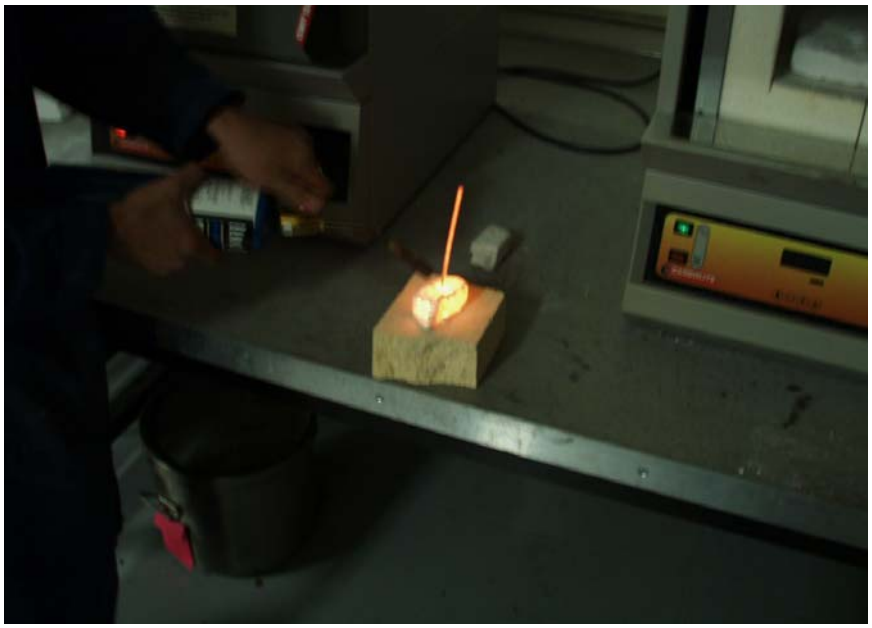

Figure 36. Glowing bricks after heating at 1200 C, as flame igniter for propane-fueled brazing torch.

7.5. Summary of Combustion Study

The following conclusions and considerations can be drawn from the experimental study:

1. With the current experimental procedure, successful spark generations did not ignite combustion or flame from the various combustible mixture investigated. Qualitatively the light intensity of the sparks was considered insufficient to activate a combustion reaction of mixtures, which would otherwise ignite when flint sparks (with qualitatively higher light intensity) were generated.

2. The combustible mixtures ignited with the generation of electric sparks possessing spark intensity lower than flint sparks. This observation suggests that, given sufficient time for heat exchange and reaction activation to take place, combustion could be ignited with relatively low temperature sparks.

3. Flame was not ignited during steel grinding which sent sparks into an air-propane mixture suitable for brazing process. In contrast to the case of electric spark, high velocity of steel grinding sparks might prevent the combustible mixture from having sufficient time for heat exchange and reaction activation.

4. Flame ignition in the gasoline vapor-air mixture was not observed in any kind of spark generations (impact/flint/electric). This observation was in a reasonably good agreement with established data regarding the very narrow range of combustible mixtures of such a substance (29,30). The environment achievable during experiments in this study was considered unsuitable for combustion testing for gasoline vapor-air mixture.

5. Flame was ignited on gasoline-wet filter paper when sparks from flint or electricity contacted the paper. Immediate contact between impact sparks and the wet filter paper was not verified due to difficulties in high speed camera recording. However, it was assumed that such direct contact occurred because the filter paper was placed directly on the target surface. In contrast to the case of flint and electric sparks, sparks generated by steel grinding did not ignite flame even though they contacted the gasoline-wet filter paper. Because the intensity of the steel grinding sparks is lower than that of flint sparks, temperature of sparks was considered to be the main factor in this flame ignition. On the other hand, electric sparks, with lower intensity than that of flint sparks, ignited flame, possibly due to the larger thermal mass that each electric spark carried.

8. CONCLUSIONS

Phase 1: Thermodynamic analyses to evaluate possible reactions for sparking.

- The most reactive combination of constituents was found to be between dry-rust and aluminum, which has an ignition temperature of 900 ^{o}C.

- With the above ignition temperature, it was predicted that an impact incident with a threshold energy level of 90-100 Joule/cm^2, for an aluminum coating of 250 μm thick, will produce sparks.

Phase 2: Impact testing between rusted/clean projectile and Al-coated steel target.

- Sparks were generated during impact between rusted steel projectiles and Al-coated steel.

- The threshold impact incident to initiate sparking was shown to be corresponding to a 75 gram rusted projectile hitting the Al-coated steel with a velocity of 12 m/s. This threshold impact incident corresponded to an impact energy density of 50 to 75 Joule/cm^2 absorbed by the 250 μm thick aluminum coating.

- Sparks could also be generated with only rust and steel impact (without aluminum coating). However, the aluminum coat on steel enhanced the spark generation allowing it to occur at lower threshold energy and with higher intensities.

- Water content on rust was found to reduce susceptibility of sparking in both Al-coated and uncoated steels. However, when the rusted steel projectile was wet, Al-coated steel was found to be more spark susceptible than uncoated steel at an equal impact velocity. In the extremely wet environment, uncoated steel did not generate spark while Al-coated steel could still generate a spark, although of small to moderate intensity.

Phase 3: Combustion testing upon impact between rusted steel and Al-coated steel target.

- With the amount of rust used in the present investigation, combustion has not been initiated in propane, methane, and gasoline containing atmosphere.

- Combustion occurred in acetylene containing atmosphere at acetylene/air ratio higher than 0.25. The role of high sensitivity for pressure of acetylene to ignite combustion was not investigated.

- Verification experiments showed that the present experimental set-up did not suffer from dilution of combustible mixture during the launching of the projectile. The

absence of combustion in most of the experiment was considered a representative observation.

- Verification experiments with steel grinding and a heated object as a possible flame igniter for propane-fueled brazing torch showed that there are other factors necessary for flame ignition that could not be attained or generated during the impact study. These factors include the larger amount of thermal mass (larger amount of sparks), sufficient time for heat transfer, and reaction activation.

REFERENCES

1. Hoseong Lee, "Summary of Two Papers: 'Thermite Sparking in the Offshore Environment' and 'Aluminum-Coated Steel: Sparking and Fire Hazard'," ABS Internal Memorandum (10 March 1999)
2. Health and Safety Laboratories, "Frictional Sparking Risks with Light Metals and Alloys," Technical Information Leaflet.
3. S. Ramberg, "Safety Aspects Regarding Use of Aluminum in Offshore Structures, "Det Norske Veritas Reports, Proceedings of the Fourth Symposium of Materials Science, Norwegian Institute of Technology, Trondheim, Norway, August (1986).
4. R. T. Roderburg, S. Mann, B. Viij, P. K. Anderson, D. Schinstad and T. E. Foyn, "Aluminum Office: Safety Analysis", DNV Report 85, 3208, DNV, Hovik, Norway (1985).
5. R. T. Roderburg, "Offshore Use of Aluminum; Rules and Regulations for Passive Fire Protection", Veritas Report No. 83-0495, DNV, Hovik, Norway (1983).
6. B. L. Chun, "Explosion Test of Hot Dip Aluminizing," Report submitted by Ship Design Office, Hyundai Heavy Industries, Co. Ltd., June 1 (1997).
7. T. E. Foyn and J. L. Moe, "Ignitions of Explosive Gases by Aluminum Alloy or Steel Drop Weight Hitting Rusted Steel, "Aluminum Offshore Project Report No. 1.2, (Veritec report No. 85-3407, (1985).
8. J. Havel, "Aluminum Coatings," Private Communication, to ABS, March 11, (1999).
9. Editor, "Aluminum-Coated Steels: Sparking and the Fire Hazard," Metals and Materials, pp. 26-27, October (1976).
10. E. Hay and R. Adermann, "Thermite Sparking in the Offshore Environment," SPE paper #16548, Soc.of Pet. Eng., (1987).
11. J. C. Bailey, "Frictional Sparking of Aluminum", The Institute of Mining Engineers, Trans AIME-SME, Vol 118, part 4, pp.223-240 (1959).
12. D. Rae, "The Ignition of Gas by the Impact of Light Alloys on Oxide-Coated Surfaces", Ministry of Power, S. M. R. E. Research Report #177, UK, (November 1959).
13. G. L. Kehl, "The Spark Test," The Principles of Metallographic Laboratory Practice, pp. 312-315, McGraw-Hill, NY, NY (1949).
14. ASM International, ASM Handbook, "Scrap Use by Industry," Properties and Selections: Iron, Steels and High Performance Alloys, Vol.1, pp. 1028, ASM, Materials Park, OH, (1990).
15. ASM International, "Aluminum-Base Coatings," Metals Handbook: Corrosion, Vol. 13, pp. 527-528, 1014, ASM, Materials Park, OH, (1987).
16. ASM International, "Aluminum-Coated (Aluminized) Steel", Metals Handbook: Corrosion, Vol. 13, pp. 434-436, ASM, Material Park, OH, (1987).
17. ASM International, "Hot Dip Aluminum Coatings", ASM Handbook: Surface Engineering, Vol. 5, pp. 717-720, ASM, Materials Park, OH, (1992).

18. R. Brenna and R. Hays, " Thermal Spray Coating for Marine Corrosion Control", Proceedings of SSPC '95, Protective Coating, Steel Structure Painting Council Conference, pp. 94-102 (1995).

19. M. Jacobson, A. R. Cooper and J. Nagy, " Explosibility of Metal Powders", Report RI 6516, U. S. Dept. of Interior, Bureau of Mines, Washington, D.C. (1974).

20. ASM International, "Aluminum Powder," Metals Handbook: Powder Metallurgy, Vol. 7, ASM, Materials Park, OH, pp.129-130 (1984).

21. C. J. Dahn, "Explosivity and Pyrophoricity of Metal Powders", Metals Handbook:: Powder Metallurgy, Vol. 7, ASM International, Materials Park, OH, pp. 194-200 (1984).

22. H. H. Uhlig, Corrosion and Corrosion Control, pp. 92-94, John Wiley, NY, 2nd edition, (1971).

23. J. Wu, "Thermite," Encyclopedia Britannica, Vol. 21, pp. 1009-1010, (1966).

24. M. A. Meyers, "Shock-Induced Chemical Reactions", Dynamic Behavior of Materials, Section 8.7, pp 218-228, John Wiley, NY (1994).

25. N. Gryadunov, A. S. Shteinberg, and E. A. Dobler, "Initiation of a Chemical Reaction in a Titanium-Carbon Powder Mixture by High-Velocity Impact", Doklady Akademic Nauk., Vol. 321, pp 825-96, (1991).

26. T. J. Ahren, "Equation of State", High-Pressure Shock Compression of Solids, Chapter 4, pp 75-113, Springer-Verlag, NY (1992).

27. Y. Horie, "Shock-Induced Chemical Reactions in Inorganic Powder Mixtures", Shock Waves in Materials Science, Chapter 4, pp. 67-100, Springer-Verlag, NY (1993).

28. D. E. Grady and M. E. Kipp, "Dynamic Fracture and Fragmentation", Shock Waves in Material Science, Chapter 8, pp. 265-322, Springer-Verlag, NY (1993).

29. Coordinating Research Council, "Handbook of Aviation Fuel Properties", "Flames ability and Ignition Characteristics", pp. 70-71, 74-75, 78, 83, Society of Automation Engineers, Warrendale, PA, (1983).

30. W. A. Affens, "Flammability Properties of Hydrocarbon Fuels", J. of Chemical and Engineering Data, vol 11(2), pp 197-202 (1966).